THEORETICAL AND PRACTICAL ASPECTS OF 2D SHAPE ASSESSMENT USING SELECTIVE FIXATIONS

by
HÜLYA YALÇIN
BS. in E.E., Boğaziçi University, 1996

Submitted to the Institude for Graduate Studies in
Science and Engineering in partial fullfillment of
the requirements for the degree of
Master of Science
in
Systems and Control Engineering

Boğaziçi University
1999

THEORETICAL AND PRACTICAL ASPECTS OF 2D SHAPE ASSESSMENT USING SELECTIVE FIXATIONS

APPROVED BY:

Assoc. Prof. H. Işıl Bozma ……..
(Thesis Supervisor)

Prof. Dr. Aytül Erçil ……..

Prof. Dr. Bülent Sankur ……..

DATE OF APPROVAL: February 2nd, 1999

ACKNOWLEDGMENTS

I am very grateful to my thesis supervisor Assoc. Prof. H. Işıl Bozma, who initially introduced me the subject, for her continuous support, guidance and laboratory facilities she provided from the beginning of this work. Working with her was a good opportunity for me to learn how to conduct scientific research.

I would like to express my gratitude to Prof. Bülent Sankur and Prof. Aytül Erçil for reading my thesis in a short period of time and being member of my thesis jury. I would like to thank Prof. Yorgo İstefanopulos for his final touch on my thesis.

I want to express my special thanks to my friends Turhan Alnıtemiz and Koray Çiftçi for their help.

Finally I would like to thank my family. They were so patient towards me and they supported me at every stage of my work.

THEORETICAL AND PRACTICAL ASPECTS OF 2D SHAPE ASSESSMENT USING SELECTIVE FIXATIONS

ABSTRACT

In this thesis, we present a mathematical framework for selective fixation generation and its usage through artificial potential functions.

Recent research suggests that computational advantages may be realized for vision problems when cameras are capable of fixating on areas of interest. Studies on the formalization of the task of selecting a sequence of fixation points and saccade directions that efficiently examine the area being searched have been limited. In our earlier work, we have developed a simple heuristic algorithm based on simple computations on the periphery region of current fixation point to determine a new visual target. The MS research presented here aims to construct the underlying theory of selective fixation control using artificial potential functions.

We implemented the approach on BUVIS, an inspection system endowed with visual attention capability. Experiments demonstrating the robustness to lighting conditions and real-timeness of the system are presented for industrial objects with varying illumination conditions.

SEÇİCİ ALGI KULLANILARAK İKİ BOYUTLU ŞEKİL TANIMANIN TEORİK VE PRATİK ANALİZİ

ÖZET

Bu tezde, seçici algı ile sabitlenme noktaları dizisi oluşturulması ve bu dizinin şekil tanıma işleri için kullanımı, yapay potansiyel fonksiyonlar kullanılarak matematiksel bir çerçevede incelenmiştir.

Yakın zamandaki çalışmalar, seçici algılamanın tanıma işlemlerinin gerçek zamanda uygulanabilirliğini önemli ölçüde arttırdığını göstermektedir. Fakat seçici algının temelini oluşturan sabitlenme noktaları dizisinin oluşturulmasının formülasyonu konusunda sınırlı sayıda teorik çalışma yapılmıştır. Önceki çalışmalarımızda, hali hazırdaki sabitlenme noktasının etrafında basit hesaplamalar yaparak bir sonraki sabitlenme noktasını belirleyen buluşsal bir algoritma geliştirilmişti. Sunulan tez, bunu - sabitlenme noktaları dizisinin oluşturulması ve kullanılması- matematiksel bir çerçevede yapay potansiyel fonksiyonları kullanarak gerçekleştirmektedir.

Çalışmamız BUVIS -görsel algı yeteneği olan bir denetleme sistemi- üzerinde uygulamaya geçirilmişti. Sistemin değişik ışıklandırma koşullarındaki performansı ve gerçek zamanda uygulanabilirliği, endüstriyel nesneler kullanılarak yapılan deneylerle irdelenmiştir.

TABLE OF CONTENTS

LIST OF FIGURES

LIST OF TABLES

LIST OF SYMBOLS

C	Set of all pixels
C x C	State space
f_1	Vector field that is negative gradient of the map F_1 with respect to x
F	Artificial potential function
F_1	A scalar valued map on the state space
I	The image intensity function defined on C
$\nabla I(\underline{x})$	Intensity gradient at the point $\underline{x}$
J	90^o rotation operator
O_i	Obstacle space for F_i
Q	Maximum of q, r, and s
u	Vector between $\underline{x}$ and $\underline{x}_o$
v	Vector between $\underline{x}_f$ and $\underline{x}$
$\underline{x}_o$	Current location
x^k	Current fixation point
(x,x^k)	A candidate point in the state space given the current fixation point x^k
β_1	Product of the various obstacle functions
β_{11}	Term that marks points where the image gradient vanishes as obstacles
β_{12}	Term that ensures the saccade direction is close to the directional cue
β_{13}	Ensures that next fixation point is within the vicinity of current fix. point
γ_2	Potential well for F_2
φ_{2mn}	Quotient function
φ_{1pqrs}	Quotient function
σ	Squashing function
σ_d	Sharpening function

1. INTRODUCTION

In machine vision, there is a growing trend towards goal-oriented systems, where effectiveness in the world is taken as a structuring constraint in designing systems [1]. With this philosophy, the need to manage resources more efficiently has become a crucial feature for vision systems operating in real-time dynamic environments. A system using real-world visual input for decision-making must ignore the irrelevant visual stimuli, attend to the salient image points and place reliable priorities on tasks and resources. Such work must confront the issues of deciding what to perceive "next".

Traditionally, research in machine vision has concentrated on thorough analysis of acquired images. This contrasts with human perception. For human visual behaviour, selectively gathering information about the environment is characterized by the ability to fixate on a point of interest and the ability to select new fixation locations [2]. Humans can shift the attention by concentrating on a part of the field of view. Motivated by human visual system, recent studies in machine vision have tried to mimic this behaviour. These studies depend on detection of visual targets and interrogation around those targets instead of processing whole image. The process of identifying and selecting new visual targets is referred to as selective fixation control [3]. Remarkable efficiency on computational grounds has been observed in machine vision systems motivated by fixation control [4].

In this manner, visual resources are allocated to process only a small part of the whole scene [5,6]. In our earlier work, we have devised a visual inspection system - based on a simple heuristic algorithm - which selectively fixates on the interesting parts of an incoming image and uses the attentional sequence thus gathered in a task-dependent manner - specifically the task of tracing an object's outline [7,8,9]. In this thesis, we present a unified mathematical framework based on artificial potential functions - which formalizes this algorithm. It turns out that this formalism tantamounts to a feedback based approach - that naturally leads to the automatic generation of camera actuator commands that cause the camera to find a sequence of fixation points and use the attentional sequence thus generated a in top-down driven task - such as the tracing of salient parts of the objects. In contrast to open loop, process-all systems, the provable correctness of such a closed loop system can be investigated.

1.1. Literature Survey

In following sections recent studies in selective attention, inspection and artificial potential functions are reviewed.

1.1.1. Selective Attention

The process of "looking" at a single point in the three dimensional scene is known as "fixating", and the location at which the eyes (or equivalently, cameras) are aimed is known as the fixation point. Recent research suggests that computational advantages may be realized for vision problems when cameras are capable of fixating only on an object of interest [2,10,11]. The process of identifying and selecting new visual targets is referred to as selective fixation control.

Vision systems based on selective perception are often modeled based on attributes of the human visual system since this is the most well-studied visual system. Two particular attributes, ocular motion and foveal-peripheral vision, have proven to be essential.

Ocular motion allows "saccadic" movement of the eyes to direct the point of the visual field [12]. The saccadic eye movement system is responsible for directing the fovea to a region of interest in the visual field rapidly. Saccades take place at very high speeds and are thought to be partially controlled by the cerebral cortex and partially by the superior colliculus which receives low and high level visual information from the retina and the visual cortex respectively.

Foveal-peripheral vision enables humans to perceive small regions in fine detail in combination with a wide field of view at coarse detail [13]. Though its effect on higher levels of processing is not clearly understood, this fovea-periphery distinction in the retina brings about the need for moving the optical axis to regions of interest for detailed processing [5,14,15,16].

Motivated by the findings in biological studies, vision systems allocate their resources to process only the most relevant parts of the incoming data. The central issue in selective vision is sequential decision making. For a given scene and sensing goal, what is the strategy for selecting new fixation points? For several of these systems, this involves

the movement of one or more cameras so that the new visual targets are fixated. In a few cases cameras do not move, but the system attends to the new target in the image by computational or windowing methods.

Koch and Ullman describe a mechanism for shifting attention across the visual field based on an abstract measure of "saliency" [17]. The method assumes that any number of elementary features (such as color or orientation) are available from computations performed in parallel across the entire image. For each image location, a quantitative measure of saliency is obtained through a combination of the low-level feature values at that location. The maximum value in the resulting saliency map is then chosen as the next visual target. Attentional shifts can occur as the image changes, or by dynamically altering the relative weightings of different feature types. The discussion is theoretical and strongly motivated by physiological concerns. Yeshurun and Schwartz determine the location of next fixation point by a control algorithm based on the derivative of the curve tangent to the contours, on the premise that most shape information is avaliable at points of fastest angle change[18].

Meanwhile, vision researchers have studied ways of formalizing the process of selective attention. In [1], fixation sequences are generated using augmented Hidden Markov models. They augment the usual paradigm of eye movements -as a result of sequential cognitive effort and image analysis- with a new explicit representation -an augmented hidden Markov Model- of probabilistic and task-dependent attentional sequencing. In [19,20], the fixation sequences - generated based on Belief Functions - are used in simple navigation tasks requiring recognition. Focus of attention mechanisms are discussed in [21].

Some of these methods have been tested with physical implementations [19,20,22]. Clark and Ferrier describe a physical implementation based on saliency measure to direct the movements of stereo cameras [23]. A two-level control hierarchy is used, in which the lower level is a traditional feedback control system, modeled after the human oculomotor system and capable of visual tracking. The higher level in this hierarchy is based on a realization of Koch and Ullman's saliency map to select new targets for fixation. Another implementation work, by Rimey and Brown, on the control of selective perception based on prior knowledge represented by Bayes networks and decision theory is described in [24]. The TEA-1 selective vision system described in this paper, uses Bayes nets for representation, benefit-cost analysis for control of visual and non-visual actions; and its

data structures and decision making algorithms provide a general, reusable framework. Its software framework allows design of purposive, selective vision systems and uses Bayesian networks and decision theory to control active and sufficing vision algorithms. Slowe and Marsic from Rutgers University developed a scheme for efficient compression and description of the semantic content of video and image based on selective perception [25]. The compression is based on content-correlates in a sense that we find the regions of interest (ROIs) and then compress the "sub-images" within the ROIs. Brown from University of Rochester is developing autonomous vehicles based on selective perception, especially those that perform off-road, and are asked to accomplish survey, location, detection type tasks [26]. They apply Bayes nets to the intelligent choice, tuning, and pointing of multiple sensors and the fusion of their outputs into scene interpretations that can be used to guide further scene analysis.

These approaches, although all very powerful in terms of fixation sequence generation, have been less amenable to rigorous analysis such as establishing the stable points of the system.

1.1.2. Inspection

In many industrial process control situations, the need to identify and classify defects is key to enabling process improvements. Inspection is used for this task. The driving force behind inspection is the reward to be gained from increased throughput, improved product quality and unit cost reduction [27]. In other words, providing more of a better product at a lower price.

As modern manufacturing processes become more advanced, the inspection tasks required to monitor them become more complex. As a result automated inspection is required. The benefits of automating processes are well known; humans typically suffer from fatigue, inconsistency and slowness, whereas machines offer repeatability, accuracy and efficiency [28].

Within manufacturing, automated visual inspection has been realizing at a comparatively slow pace, due to the inherent problems with respect to real-timeness and robustness [29]. In an academic research, one might obtain unsatisfactory results but be still successful if one is able to make good reasoning of the results. For an automation

system accuracy and consistency in inspection is a must. Another thing is that vision systems can process only what the cameras are able to view. Even use of multi-cameras are possible, then comes in the problem of real-timeness. Thus, the requirements of automation are: 100% inspection, consistency, higher accuracy and real-timeness. Commercial vision systems are available for a wide variety of inspection tasks including automobile, electronics, metal industries and have a taxanomy based on type of image used - binary, intensity, color and range. Intensity based systems - although of great potential - has had limited applicability in complex industrial environments. Such systems usually process the whole image and use image subtraction or localized histogramming methods for defect detection [30].

Naturally, studies in automated visual inspection are mostly affiliated by corporations and mostly concentrated on developing automated PCB inspection systems. On the other hand, some of the applications UK Industrial Vision Association -an industrial association whose objective is to promote the use of vision technology by the manufacturing industry- are working on indicate the diverse nature to which machine vision technology can be put: 2D code reading, hot product inspection, thermometer calibration, windscreen wiper development [31].

1.1.3. Artificial Potential Functions

In robotics, potential field approach has been applied to robot manipulators for dealing with the problem of operational space formulation [32]. The idea of using "potential functions" for the specification of robot tasks with a view of control problems in mind was pioneered by Khatib in the context of obstacle avoidance and Koditschek in navigation [32,33]. Since then, numerous investigators have attempted to use potential functions in various robotic applications [34,35]. They fall into three categories: First group of papers address the problem of undesired local minima [36,37,38]. Second group, view potential functions as-path planning aids. For example, the "valley tracking" technique [39], and Warren's path optimization procedure [40]. Third group of papers extend the use of potential functions to time-varying situations. For example Newman's work of avoiding moving obstacles [41] and Khatib's real-time obstacle avoidance

technique [32]. In vision literature, potential fields have been applied in numerous contents such as the derivation of medial axis transform of a 2D polygonal region [42].

1.2. General Problem Statement and Approach

The thesis aims to: 1) develop a mathematical framework for fixation control based on artificial potential functions and 2) evaluate its usage in the extraction of relevant info such as contours and certain geometric properties for shape recovery.

In this thesis, we propose to solve the problem of generation of attentional sequences and their usage in task-driven tasks by imposing artificial potential energy function on the image plane. First let us sketch the solution approach.

Let $\mathbf{C}$ represent the set of all pixels and $\mathbf{C}$ x $\mathbf{C}$ represent the state space. Note that each point (x, x^k) in the state space denotes a candidate point given the current fixation point x^k. Consider an artificial potential function $F \in C[\mathbf{C}x\mathbf{C}, R]$ constructed on the state space and such that for each $x \in \mathbf{C}$ which has a minimum at the point to be yet determined and is maximal over uninteresting points. For a given fixation point x^k, F can be visualized as three-dimensional surface.

Once a suitable F is constructed, it automatically determines a feedback control law $\tau = -D_x F(x, x^k)$, where τ is the input to be applied to the controller. It can be shown that the closed-loop actuator system inherits the critical qualitative behaviour of F's gradient trajectories (i.e. $\dot{x} = -D_x F(x, x^k)$). In our work, two artificial potential functions, F_1 and F_2, are formulated. First prominent points on the contour –a set of fixation points- are determined through potential function F_1. Following, the contour segment between each consecutive fixation points is determined through potential function F_2. Hence, the construction of these potential functions becomes a critical issue. The terms in the potential function F_1, are selected such that the pixels on the contour with features deviating from those of its neighbours are favoured as fixation points. Deviation assessment is based on rapid direction change and irregularity - therefore high information content. In order to ignore irrelevant data, fixation points must be as far as possible. The terms in the potential function F_2 are selected such that an optimal path between successive fixation points is traced along the edge pixels.

Once generated and connected, these fixation points then serve as the points chosen on the object that form a rough skeleton of the contour. These points are then grouped together. Finally, we compute elliptic Fourier coefficients of the contours detected in order to extract features. In many applications of pattern recognition and digital image processing the shape of an object is represented by its contour. Fourier descriptors provide a means to characterize contours. The idea is to represent the contour as a function of one variable, expand the function in its Fourier series, and use the coefficients of the series as Fourier descriptors. Having represented shape features by Fourier descriptors, an Euclidean-invariant graph composed of the features of the object is constructed for fast comparison of object features.

1.3. Contributions of the Thesis

The contributions of this thesis can be summarized as follows:

1) We have constructed selective fixation control – namely, generation of attentional sequences and shifting attention - in a theoretical framework via potential functions. Both generation of fixation points and their usage in task - driven tasks are solved by imposing artificial potential energy function on the image plane.

2) We have implemented our novel theoretical method - online and reliable –within BUVIS for the analysis of complex parts.

1.4. Outline

This thesis consists of five separate chapters: A review of the literature on selective fixation control, automated visual inspection and energy-based methods is given in Chapter 1. The general overview of the original work is presented in Chapter 2. In Chapter 3, mathematical formulation of the approach is presented.

Experimental results is presented in Chapter 4. Finally Chapter 5, summarizes the work of this thesis and offers a few conclusions and suggestions for further work.

2. GENERAL FLOW OF PROCESSING

Our general algorithm aims to assess the shapes of objects with multiple parts. The shape assessment is achieved via extracting the contours of the object and its subparts. The contours are derived based on selective fixation control ideas combined with artificial potential functions. We implemented the approach on BUVIS, an inspection system endowed with visual attention capability. The flow of visual processing is as shown in Figure 2.1.

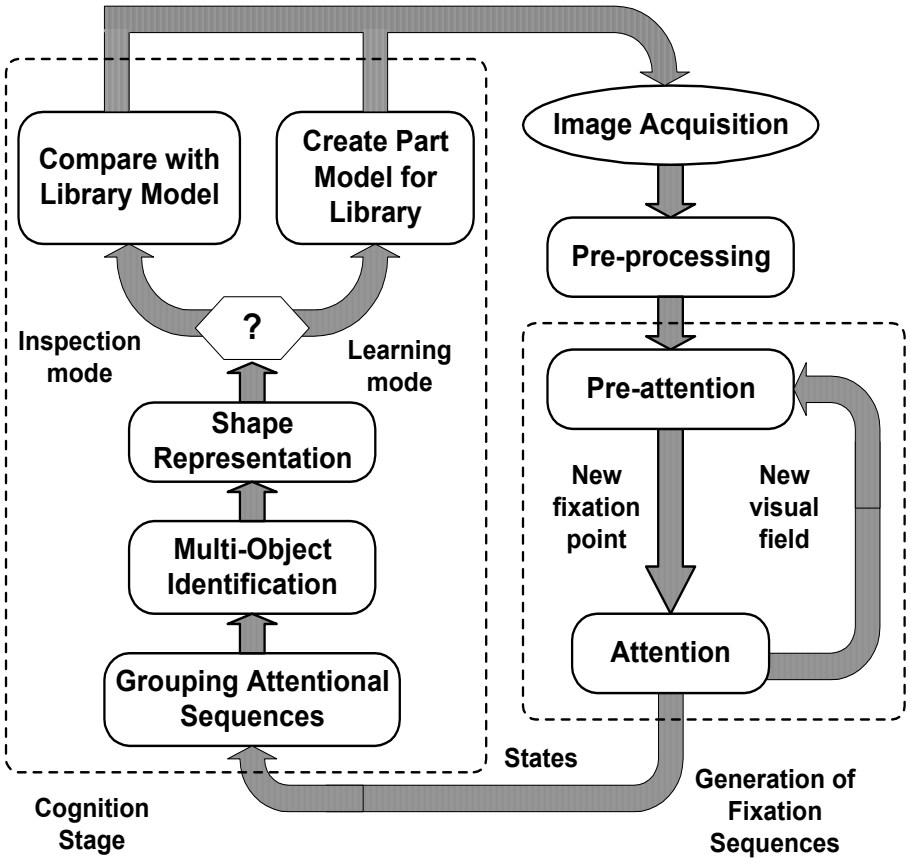

FIGURE 2.1 Flow diagram of the visual processing.

First, the incoming image is subjected to preprocessing with two purposes in mind: 1.) Removal of image noise via low-pass filtering and 2.) Extraction of prominent edges via high-pass filtering and thresholding. In our application, a very simple averaging

operator - box filter - is used for noise removal due to its computational simplicity and Sobel edge operator for edge extraction. Typical results are as shown in Figure 2.2.

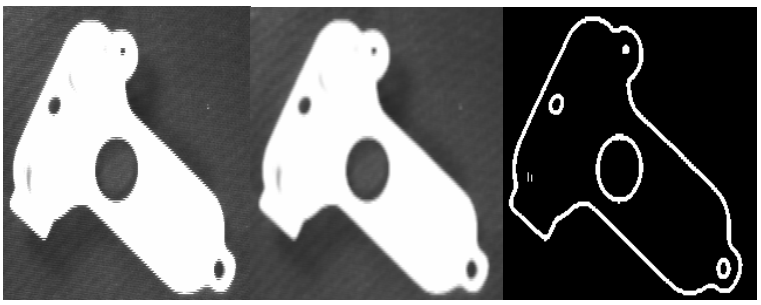

FIGURE 2.2 (Left) An industrial object - door part manufactured for automobile industry; (Center) Image after low-pass filtering; (Right) Image after edge extraction.

The next three stages constitute the maincore of the visual processing: pre-attention, attention and cognition involving spatio-temporal reasoning as shown in Figure 2.1. The aim of the pre-attention stage is to determine where to look next in the visual field. Let us observe that once the initial fixation point is determined, visual resources are allocated to process only a small part of the whole scene. After the occurrence of physical attention – i.e. the repositioning of the current fixation point to the newly determined fixation point- this region is subjected to further processing in order to extract more complex features. These two stages of vision occur repeatedly – collecting data in space and time and contribute to the pool of information used by the third stage to accomplish the given inspection task [19,20]. Only certain interesting points 'fixation points' are focused on and the sequence of fixation points thus generated represents a salient contour segment in a spatio-temporal manner. This fixation points serve as anchor points for further processing. As the contour of a part or a sub-part may be seen as broken into several salient contour segments due to illumination and viewing artifacts, construction of complete contours is transformed to that of merging fixation point sequences. Once merging is completed, the contour of each part or subpart is defined coarsely. Since we need accurate shape information for inspection purposes, each fixation point sequence is then used to interpolate the contour precisely. Following, elliptic Fourier descriptors (EFD) are used to compute the Euclidean shape invariants. The advantage of this representation is that the spatio-temporal representation of the contour can be used in a straightforward-manner to

compute the shape parameters. Two possible modes exist in final stage of cognition: 1.) Learning, where the system assumes that it is presented with an ideal part and forms a library model of the part; and 2.) Inspection, where the system compares the part-being-inspected to the library model and determines whether the part is faulty or not and if faulty, what the faults are.

2.1. Generation of Fixation Sequences

The aim of this stage is to determine all the salient contour segments. A salient contour segment is represented by a chain of fixation points. To start visual processing, an arbitrarily chosen edge point - in our case the upper left most edge point - is taken to be initial fixation point of the first salient contour segment. Once an initial fixation point is determined, a find-next-fixation-point procedure is continually invoked to form a chain of fixation points.

2.1.1. Pre-attention

The aim of this stage is to determine the next location to be processed and then shift processing from the current to the next selected location. The location of fixation points are of critical importance since they are utilized in order to reduce visual input data. They should be located at points where critical change occurs in visual data. In the case of contour following, it can be intuitively inferred that the fixation points should be placed more densely in regions of high contour curvature and less densely in regions of low contour curvature.

In our work, the next fixation point is determined automatically within a mathematical framework of artificial potential functions. The construction of the potential function is determined considering features important for positioning the fixation point. The construction of potential function is described in Section 3.2, and the critical points of the resulting potential field are used to estimate next

fixation point. The path that leads to next fixation point is found by following force field of the potential field, thus avoiding two dimensional search.

Having determined next fixation point, the current fixation point should be shifted from the current to the next selected location. Simply a path that leads to next fixation point starting from current fixation point is to be constructed. Since this path will be constructed between every two successive pair of fixation points, at the end the outline of the object will be traced. Even this simple task requires another level of processing - since the trajectory generated in the course of finding the next fixation point will be jagged and nonoptimal. However, taken from another perspective, this problem turns out to be a straightforward navigation problem - where the goal is to move from the current fixation point x^k to the next x^{k+1} optimally. Fixation points guide pretty well in constructing a thinner contour of an object out of edge pixels. The mathematical formulation for tracing the outline of the objects is described in section 3.3 in detail.

2.1.2. Attention

In the attentive stage, the properties which characterize the state of the fixation points are extracted. The feature vector obtained in this way is then added to the attentional sequence. The type of processing during attention is determined by the task at hand and is much more detailed in nature than that of the pre-attentive stage. In our case, we use edgetype as the feature. Edgetype is a valued entry embodying the angular attitude of the vector pointing from the current fixation point to next fixation point.

The information embodied in edgetype is used to segment the object whose attentional sequences is being generated. As soon as the next fixation point is added to the attentional sequence, the edge pixels between current and next fixation point -- the ones in the window along the direction of the vector pointing from the current fixation point to the next fixation point- are added to the segment to which fixation point belongs.

While the contour of the object is being traced, the edge pixels on the way should be segmented so that a region is not processed twice or more. Furthermore, this segmentation process is necessary for deciding whether to initialize the segmentation of

another object or not. The number of pixels segmented around each fixation point is used as a feature to decide whether the current fixation point is actually last fixation point of that segment or not. If there are no pixels to be segmented around the fixation point, then it is the last fixation point. The process of determination of initial fixation point of a new segment can be initialized.

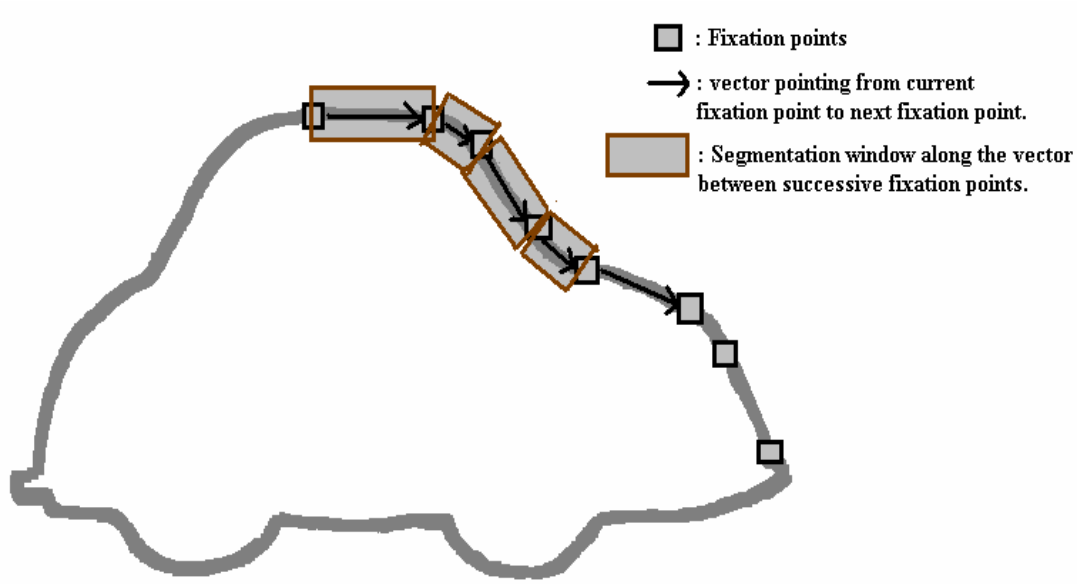

FIGURE 2.3 Segmentation process occurs while tracing the object's outline.

A window between successive fixation points grows along the saccade direction of current fixation point in order to segment the edge pixels and the edge pixels connected to current fixation point is appended to the segment as shown in Figure 2.3.

2.2. Cognition based on Fixation Points

In the cognition stage, the attentional sequences thus generated are subjected to further processing. An attentional sequence corresponds to a spatio-temporal representation of the image – since it not only represents the locations of the features, but also the manner in which they were traversed. Using attentional

sequences, an object is represented for visual recognition as a "feature ring" -- a time-ordered sequence of features perceived at each fixation, along with positions and memory traces that link the fixations as Yarbus suggested [43]. Features, in turn, are defined as being the most information contentful parts of the image.

First the sequences are grouped together if there is evidence that they belong to same subpart. The sequence represents the skeleton of the subpart. The shape invariants of each subpart are computed then a part model is constructed that represents where all the subparts are located on the part.

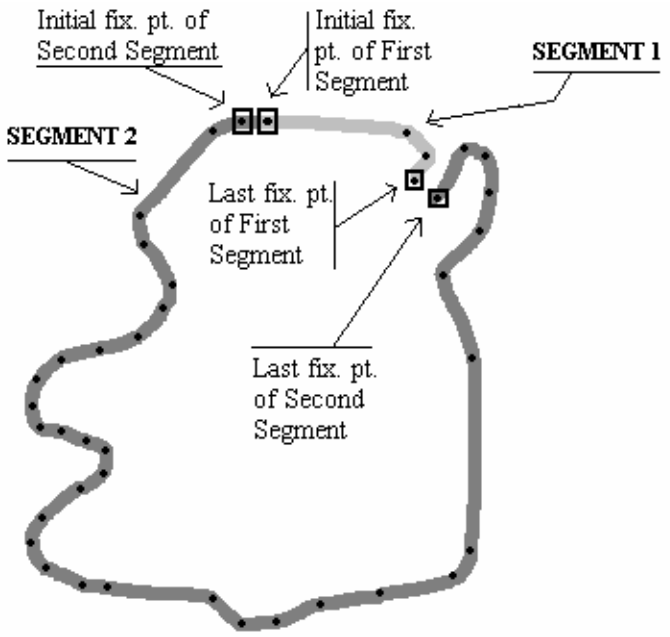

FIGURE 2.4 Merging of attentional sequences is illustrated.

2.2.1. Grouping Attentional Sequences

The first type of cognitive processing aims to group attentional sequences together. The necessity of this processing is due to the fact that when merging the segments that actually belong to the same object may be segmented as two different objects due to illumination. In particular, two segments are possibly to be grouped if their end-points are close to each other. However, this is not an easy task. Fortunately, the representation of the

segment as a chain of fixation points also provides such information approximately. The initial and the end fixation points may be taken roughly to be the end points of the segment and assessment of closedness of two segments can be made based on their physical and feature proximity, as shown in Figure 2.4. In our case, we use distance as a measure. Fixation points are aided to further serve as the points chosen on the object that somewhat forms the skeleton of the object.

2.2.2. Shape Representation

The representation of shapes is based on elliptic Fourier descriptors [44,45]. Elliptic Fourier descriptors represent a shape weighted sum of ellipsoids. Using elliptic Fourier descriptors, each shape i is defined by a vector $p_i \in P \subseteq \Re^{4k+2}$ where k is the number of harmonics:

$$p_i = \left[a_{i0} b_{i0} a_{i1} b_{i1}, c_{i1} d_{i1} \ldots a_{ik} b_{ik}, c_{ik} d_{ik}\right]^T \tag{2.1}$$

The order of harmonics k represents the accuracy of the model. The set of n shapes is then described by $p \in P \subseteq \Re^{n(4k+2)}$ via concatenating p_i [46]. The parameter set a_{ik}, b_{ik}, c_{ik} and d_{ik} can be used to extract geometric features such as major and minor axis length, orientation. Furthermore, geometric relations within and between shapes can be easily formulated mathematically. Finally, given a sequence of points forming a complete contour, a simple procedure can be used to compute the elliptic Fourier parameters [45].

$$a_n = \frac{T}{2\pi^2 n^2} \sum_{p=1}^{K} \frac{\Delta x_p}{\Delta t_p} \left(\cos \frac{2n\pi t_p}{T} - \cos \frac{2n\pi t_{p-1}}{T} \right) \tag{2.2}$$

$$b_n = \frac{T}{2\pi^2 n^2} \sum_{p=1}^{K} \frac{\Delta x_p}{\Delta t_p} \left(\sin \frac{2n\pi t_p}{T} - \sin \frac{2n\pi t_{p-1}}{T} \right) \tag{2.3}$$

$$c_n = \frac{T}{2\pi^2 n^2} \sum_{p=1}^{K} \frac{\Delta y_p}{\Delta t_p} \left(\cos \frac{2n\pi t_p}{T} - \cos \frac{2n\pi t_{p-1}}{T} \right) \tag{2.4}$$

$$d_n = \frac{T}{2\pi^2 n^2} \sum_{p=1}^{K} \frac{\Delta y_p}{\Delta t_p} \left(\sin \frac{2n\pi t_p}{T} - \sin \frac{2n\pi t_{p-1}}{T} \right) \qquad (2.5)$$

Δx_p and Δy_p are incremental changes of the contour in x and y directions during the time Δt_p. T is the period to trace the contour once. n is the harmonic number. For subpart contour, shape coefficients using fifteen harmonics are computed as illustrated in Figure 2.5.

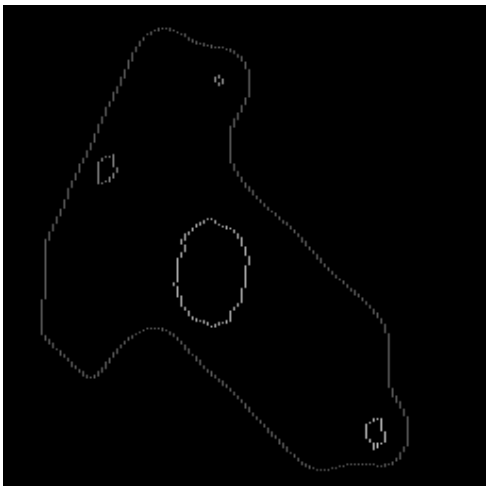

FIGURE 2.5 Contour reconstructed for industrial object out of 15 efd coefficients.

2.2.3. Construction of Part Model

Once the shape descriptors are extracted, the next stage is to examine all the subparts on the part and then construct a part model that represents where all the subparts are located on the part. Note that as the part is randomly positioned and oriented, this is not an easy task. We use shape invariants [44] for representing each sub-part and then use a particular -Euclidean-invariant subparts graph for constructing the complete part model. For shape invariants, we use the major and minor axis lengths of the ellipses passing roughly through the contour of each subpart as computed based on elliptic Fourier

descriptors. To construct our Euclidean-invariant subparts graph, we first compute the vector anchored at the center point of the part in the direction of the center point of a subpart which is assumed to be always present, use this vector to generate a rotated x-y coordinate frame and calculate the radial coordinates (r_{pi}, θ_{pi}) of the center point of each subpart i=1,..,N where N is the number of subparts as shown in Figure 2.6.

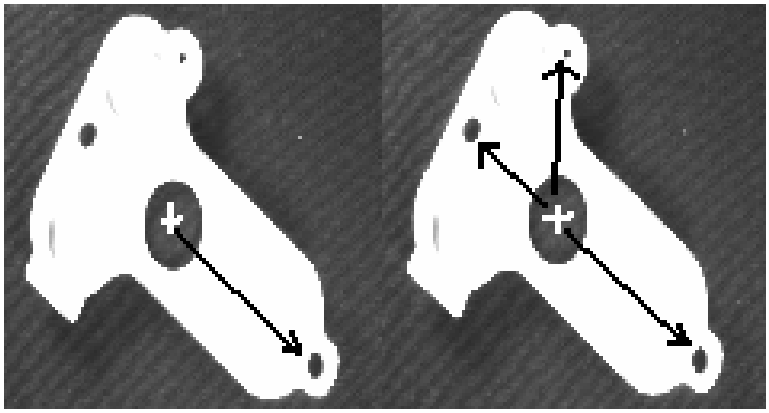

FIGURE 2.6 (Left) Reference vector, (Right) Euclidean-invariant graph.

2.2.4. Decision Stage

The decision stage has two modes. In the learning mode the system is presented with a non-defective part. Part's model is constructed and then stored in a library file to be later used. In the inspection mode, a "to-be-inspected" part is presented to the system and a decision regarding whether the part is defective or not is made. If found defective, the defects are listed. In order to accomplish this task, a model of the part is constructed and then compared with the model of the 'ideal' part. The comparison is based on identifying corresponding subparts on each part respectively and then using a measure of proximity to determine whether the positioning and shape of each subpart on the inspected part is as it should be. In our Euclidean-invariant graph representation of the parts, a mere comparison in radial coordinates suffices to identify corresponding subparts. The j'th subpart on the model is matched with the i'th subpart on the part being inspected that minimizes the Spatial-Similarity-Criterion, SSC_{ji},

$$SSC_{ji} = \left[\left(r_{pi} * \cos(\theta_{pi}) - r_{mj} * \cos(\theta_{mj})\right)^2 + \left(r_{pi} * \sin(\theta_{pi}) - r_{mj} * \sin(\theta_{mj})\right)^2\right]^{\frac{1}{2}} \quad (2.6)$$

Here, r_{pi} and r_{mj} are the radial distance of i'th subpart of to-inspected-part and j'th subpart of model part to the starting point of the reference vector respectively and θ_{pi} and θ_{mj} are the angular displacements of corresponding subparts relative to the reference vector. The average SSC_{ji} for all subparts, is defined as follows,

$$ASSC = \frac{1}{N}\sum_{j}^{N} SSC_{j(\text{subpart\_on\_inspected\_one\_mathced\_to\_}j^{th}\text{\_subpart\_on\_model})} \quad (2.7)$$

can be used as a feature to determine if a subpart is missing. The ASSC value is almost invariant for a part no matter what its orientation is. Due to a missing subpart (i.e. a missing hole), the value of ASSC will change considerably compared with the model's ASSC. Having determined that there exists a missing subpart, the missing subpart can easily be identified through SSC_{ji} values.

Having matched the segments on both images, our next objective is to determine whether the segments are properly shaped within some tolerance. The invariants computed out of first few harmonics successfully aids in rough inspection of the shape of the segments.

2.3. Discussion

We have implemented these ideas in the primary stage of BUVIS development – an experimental testbed for this work. This work is presented in [7]. In the decision making stage regarding the status of the inspected part, we solved matching problem based on SSC feature and Euclidean invariant graph. The asssumption is that there should exist two invariant points on the part being inspected. Then the subparts on the part being inspected and the subparts on the model part can be correctly matched for further inspection. We further assume that the parts are being viewed from invariant view direction orthographically and the distance of camera does not change. The parts to be inspected can

be viewed at any orientation, that is, Euclidean invariant graph is almost independent of rotation. We use ASSC feature to assess the performance of our system. It is expected that ASSC value is almost zero if all subparts on the part being inspected matches to those of the model part and there is no misplaced or missing subpart and ASSC value is considerably different from zero otherwise. Indeed, our experiments have verified this expectation. We have observed that due to the foreshortening effects, ASSC is not exactly zero but close to zero even if all subparts on the part being inspected matches to those of the model part and there is no misplaced or missing subpart. Let us remark that in case of a part with acceptable many subparts and a faulty part, this ASSC definition may not yield good results. Since ASSC is the average of minimizing SSC values for all subparts on the inspected part, if the number of subparts on the part increases, ASSC value will hardly reflect the case that there exists a missing or misplaced subpart.

After the subparts on the inspected part and those of model part are correctly matched, the shape parameters of the mathcing subparts are compared to determine if the subparts are correctly shaped or not. Comparing only shape parameters of matching parts allows fast comparison inspected of the part to model part. Let us finally add that we have had promising results in terms of computational time. Time considerations suggest that it is possible to realize a real-time system using the presented approach.

3. MATHEMATICAL FORMULATION

In this section, we present mathematical framework based on artificial potential functions - which formalizes the algorithm of generating attentional sequences and their usage. First, the general solution approach through potential functions is sketched for both levels. Then, two artificial potentials are formulated, one for the determination of prominent points –a set of fixation points- and one for the determination of the contour segment between each successive fixation points. Theoretical stability analysis of the results is presented following the construction of potential functions for each level.

3.1. Potential Function Approach

The generation of fixation points and their usage in task-driven tasks can effectively be solved by imposing artificial potential energy function on the image plane. The solution approach can be outlined as follows:

The set of all pixels is represented by C and the state space is represented by C x C. Each point (x,x^k) in the state space denotes a candidate point given the current fixation point x^k. An artificial potential function $F \in C[C \text{x} C, R]$ is constructed on the state space such that for each $x \in C$ there exists a minimum at the point to be yet determined and F is maximal over uninteresting points. F can be visualized as three-dimensional surface for a given fixation point x^k.

Once a suitable F is constructed, a feedback control law $\tau = -D_x F(x,x^k)$ is automatically determined. The closed-loop actuator system inherits the critical qualitative behavior of F's gradient trajectories (i.e. $\dot{x} = -D_x F(x,x^k)$).

We presume an artificial potential function F - a scalar valued map on the state space. Define the vector field f to be the negative gradient of the map F with respect to x

$$f(x;x^k) \equiv -D_x F(x,x^k). \qquad (3.1)$$

Here the semicolon notation is intended to call attention to the parametric role that the current fixation point x^k will play in determining the motion of the system. Motion on this subspace of the state space is governed by the limit properties of the gradient dynamical system $\dot{x} = f(x; x^k)$ whose integral curve through the initial condition x^k will be denoted by $\dot{x} = f^t(x^k; x^k)$. When $f(x^*; x^k) = 0$ implies that $D_x f(x^*; x^k)$ has full rank, it can be guaranteed that the limit set $f^\infty(x_o; x^k) = \lim_{t\to\infty} f^t(x^k; x^k)$ of every trajectory through any initial condition x^k is some isolated singularity x^* which can then be designated as the next fixation point $x^{k+1} \equiv x^*$.

3.2. Generation of Fixation Points

The aim of this stage is as follows: Given a current fixation point, determine where to look next in the image. In our earlier work, we have achieved this via applying simple computations on the periphery region of the current fixation point by considering all candidate image points, computing their saliency - a measure of interest based on the presence of simple features with low computational requirements - and designating the image point with the greatest saliency as the potential fixation point. Here, we would like to formalize this simple heuristic algorithm.

3.2.1. The Artificial Potential Function

Let us now describe the terms that appear in the potential function. Let *I* denote the image intensity function defined on C and $\nabla I(\underline{x})$ denote image gradient at the point $\underline{x}$.

Obstacle points are enclosed by three terms: First, a β_{11} term that marks those points where the image gradient vanishes as obstacles:

$$\beta_{11}(\underline{x}) = \nabla I(\underline{x})^T \nabla I(\underline{x}) \qquad (3.2)$$

Next, a β_{12} term that ensures the saccade direction ($\underline{x}$ - x^k) is close to the directional cue $\nabla I(x^k)$ at the current fixation point as:

$$\beta_{12}(\underline{x}, x^k) = \left[J\nabla(x^k)\right]^T(\underline{x} - x^k) \tag{3.3}$$

where J is the rotation operator.

Finally, a β_{13} term ensures that the next fixation point is within the vicinity of the current fixation point as:

$$\beta_{13}(\underline{x}, x^k) = (\underline{x} - x^k)^T(\underline{x} - x^k) \tag{3.4}$$

Denote the product of the various obstacle functions by β_1. The obstacle space O_1 is defined

$$O_1 = \{\underline{x} \in C : \beta_1(\underline{x}, x^k) \le 0\} \tag{3.5}$$

Constructed in a manner similar to [34,35], the artificial potential function is a three parameter family defined by the composition of three functions:

$$F_1(\underline{x}, x^k) = \sigma \circ \varphi_{1qsr}(\underline{x}, x^k) \tag{3.6}$$

where the quotient function φ_{1qsr} is defined by

$$\varphi_{1qsr} = \frac{1}{\beta_{11}^q \beta_{12}^r \beta_{13}^s} \tag{3.7}$$

the squashing function σ is defined by

$$\sigma(y) = \frac{y}{y+1} \tag{3.8}$$

Here, the functions β_{12}, β_{13}, φ_{1qsr} and F_1 are all dependent on x^k but for the simplification of the notation, the second argument x^k will be omitted in the sequel .

Note that the height of φ_{1qsr} is maximal (goes to ∞) on the obstacles' boundary. The parameters q, r and s are used to control the shape of φ_{1qsr}. The squashing function σ maps the image to the unit interval. The initial condition is x^k. Topologically, φ_{1qsr} is equivalent to F_1.

3.2.2. Theoretical Analysis of Fixation Generation

With the terms substituted, the function φ_{1qsr}

$$\varphi_{1qsr}(\underline{x}) = \frac{1}{\left(\nabla I(\underline{x})^T \nabla I(\underline{x})\right)^q \left((J\nabla I(\underline{x}_o))^T u\right)^s \left(u^T u\right)^r} \tag{3.9}$$

Here, $\underline{x}_o = x^k$, is the current location, $\underline{x}$ is the candidate for target point. The gradient $\nabla I(\underline{x})$ is defined as,

$$\nabla I(\underline{x}) = \begin{bmatrix} I_x(\underline{x}) \\ I_y(\underline{x}) \end{bmatrix} \tag{3.10}$$

Also, let $u = \underline{x} - \underline{x}_o$.

$$u = \underline{x} - \underline{x}_o = \begin{bmatrix} x - x_o \\ y - y_o \end{bmatrix} \tag{3.11}$$

J is the a rotation operator by $\pi/2$,

$$J = \begin{bmatrix} 0 & -1 \\ 1 & 0 \end{bmatrix} \tag{3.11}$$

The proposed potential function $F_1 \in C[CxC, [0, 1]]$ is a composition of two functions:

$$F_1 = \sigma \circ \varphi_{1qsr} \tag{3.12}$$

Since φ_{1qsr} blows up at some points, to correct this undesired behaviour, the image of φ_{1qsr} is squashed by the map $\sigma : [0, \infty) \to [0,1]$ defined :

$$\sigma(x) = \frac{x}{1+x} \tag{3.13}$$

This function is defined over all the domain and is also admissible. Note that the first derivative of σ is strictly positive for x>0. Therefore, the surface properties of φ_{1qsr} are invariant under these maps.

$$F_1(\underline{x}) = \frac{1}{1+\left(\nabla I(\underline{x})^T \nabla I(\underline{x})\right)^q \left((J\nabla I(\underline{x}_o))^T u\right)^s \left(u^T u\right)^r} \tag{3.14}$$

The following technical lemmas give the formulas for the gradient and the Hessian (second derivative) of F_1 which will be used continually in the sequel.

Lemma 1: $\nabla\left(\nabla I(\underline{x})^T \nabla I(\underline{x})\right) = 2\nabla^2 I(\underline{x})^T \nabla I(\underline{x})$.

Proof: $\nabla\left(\nabla I(\underline{x})^T \nabla I(\underline{x})\right) = \nabla(\nabla I(\underline{x}))^T \nabla I(\underline{x}) + \nabla(\nabla I(\underline{x}))^T \nabla I(\underline{x})$

$$\nabla\left(\nabla I(\underline{x})^T \nabla I(\underline{x})\right) = 2\nabla^2 I(\underline{x})^T \nabla I(\underline{x}) \quad . \square$$

Lemma 2: $\nabla\left(u^T u\right) = 2u$

Proof: From the definition of u,

$$\nabla u = \begin{bmatrix} 1 & 0 \\ 0 & 1 \end{bmatrix}$$

$$\nabla\left(u^T u\right) = 2u(\nabla u)^T = 2u \,.\, \square$$

Lemma 3: $\nabla\left((J\nabla I(\underline{x}_o))^T u\right) = J\nabla I(\underline{x}_o)$

Proof: Define $J\nabla I(\underline{x}_o) = c$, a constant vector. Then $(J\nabla I(\underline{x}_o))^T u = c^T u$ and $\nabla\left(c^T u\right) = c \,.\, \square$

Lemma 4: The gradient of F_1 is,

$$\nabla F_1(\underline{x}) = -\frac{\|\nabla I(\underline{x})\|^{2q-2}\left((J\nabla I(\underline{x}_o))^T u\right)^{s-1}\|u\|^{2r-2}}{\left(1+\|\nabla I(\underline{x})\|^{2q}\left((J\nabla I(\underline{x}_o))^T u\right)^s\|u\|^{2r}\right)^2}\begin{bmatrix} 2q\left((J\nabla I(\underline{x}_o))^T u\right)\|u\|^2\left(\nabla^2 I(\underline{x})^T\nabla I(\underline{x})\right) \\ +s\|\nabla I(\underline{x})\|^2\|u\|^2 J\nabla I(\underline{x}_o) \\ +2r\|\nabla I(\underline{x})\|^2\left((J\nabla I(\underline{x}_o))^T u\right)u \end{bmatrix} \tag{3.15}$$

Proof: For the sake of simplicity, let $A = \nabla I(\underline{x})^T\nabla I(\underline{x})$, $B = (J\nabla I(\underline{x}_o))^T u$, and $C = u^T u$. Then F_1 is,

$$F_1 = \frac{1}{1+A^q B^s C^r}$$

$$\nabla F_1 = -\frac{1}{\left(1+A^q B^s C^r\right)^2}\nabla\left(1+A^q B^s C^r\right)$$

$$\nabla F_1 = -\frac{1}{\left(1+A^q B^s C^r\right)^2}\left(qA^{q-1}B^s C^r\nabla(A)+sA^q B^{s-1}C^r\nabla(B)+rA^q B^s C^{r-1}\nabla(C)\right)$$

$$\nabla F_1 = -\frac{A^{q-1}B^{s-1}C^{r-1}}{\left(1+A^q B^s C^r\right)^2}\left(qBC\nabla(A)+sAC\nabla(B)+rAB\nabla(C)\right) \tag{3.16}$$

Using results from Lemma 1, 2 and 3, and substituting into (3.16) for ∇A, ∇B and ∇C respectively,

$$\nabla F_1(\underline{x}) = -\frac{\|\nabla I(\underline{x})\|^{2q-2}\left((J\nabla I(\underline{x}_o))^T u\right)^{s-1}\|u\|^{2r-2}}{\left(1+\|\nabla I(\underline{x})\|^{2q}\left((J\nabla I(\underline{x}_o))^T u\right)^s\|u\|^{2r}\right)^2}\begin{pmatrix} 2q\left((J\nabla I(\underline{x}_o))^T u\right)\|u\|^2\left(\nabla^2 I(\underline{x})^T\nabla I(\underline{x})\right) \\ +s\|\nabla I(\underline{x})\|^2\|u\|^2 J\nabla I(\underline{x}_o) \\ +2r\|\nabla I(\underline{x})\|^2\left((J\nabla I(\underline{x}_o))^T u\right)u \end{pmatrix}$$

we get the stated result. □

Lemma 5: The minimal points of F_1 are determined by the following equation,

$$2q\left(J\nabla I(\underline{x}_o)^T u\right)\|u\|^2\left(\nabla^2 I(\underline{x})^T\nabla I(\underline{x})\right)+s\|\nabla I(\underline{x})\|^2\|u\|^2 J\nabla I(\underline{x}_o)+2r\|\nabla I(\underline{x})\|^2\left(J\nabla I(\underline{x}_o)^T u\right)u=0 \tag{3.17}$$

Proof: From optimization theory, a necessary condition for being a critical point is that $\nabla F_1 = 0$. In our case, we observe that these happen in four different cases.

$\|\nabla I(\underline{x})\| = 0$, $\|u\| = 0$, $(J\nabla I(\underline{x}_o))^T u = 0$ and

$2q\left((J\nabla I(\underline{x}_o))^T u\right)\|u\|^2\left(\nabla^2 I(\underline{x})^T\nabla I(\underline{x})\right)+s\|\nabla I(\underline{x})\|^2\|u\|^2 J\nabla I(\underline{x}_o)+2r\|\nabla I(\underline{x})\|^2\left((J\nabla I(\underline{x}_o))^T u\right)u=0$.

In the first three cases, we observe that the function F_1 becomes maximal. Hence, these cases are taken out of consideration. In the last case, $F_1<1$ implies minimality. □

Lemma 6: The Hessian of F_1 is evaluated at minimal points is,

$$\nabla^2 F_1(\underline{x}) = \frac{\|\nabla I(\underline{x})\|^{2q-2}\left((J\nabla I(\underline{x}_o))^T u\right)^{s-1}\|u\|^{2r-2}}{\left(1+\|\nabla I(\underline{x})\|^{2q}\left((J\nabla I(\underline{x}_o))^T u\right)^s\|u\|^{2r}\right)^2}\begin{pmatrix} -2q\left((J\nabla I(\underline{x}_o))^T u\right)\|u\|^2\nabla\left(\nabla^2 I(\underline{x})^T\nabla I(\underline{x})\right) \\ +4r\left(1+\frac{r}{q}\right)\frac{\|\nabla I(\underline{x})\|^2\left((J\nabla I(\underline{x}_o))^T u\right)uu^T}{\|u\|^2} \\ +s\left(1+\frac{s}{q}\right)\frac{\|\nabla I(\underline{x})\|^2\|u\|^2 J\nabla I(\underline{x}_o)(J\nabla I(\underline{x}_o))^T}{\left((J\nabla I(\underline{x}_o))^T u\right)} \\ +\frac{2rs\|\nabla I(\underline{x})\|^2\left((J\nabla I(\underline{x}_o))u^T\right)}{q} \\ +\frac{2rs\|\nabla I(\underline{x})\|^2\left(u(J\nabla I(\underline{x}_o))^T\right)}{q} \\ -2r\|\nabla I(\underline{x})\|^2\left((J\nabla I(\underline{x}_o))^T u\right)I_{2x2} \end{pmatrix}$$

(3.18)

Proof: Recall that ∇F_1 is

$$\nabla F_1(\underline{x}) = -\frac{\|\nabla I(\underline{x})\|^{2q-2}\left((J\nabla I(\underline{x}_o))^T u\right)^{s-1}\|u\|^{2r-2}}{\left(1+\|\nabla I(\underline{x})\|^{2q}\left((J\nabla I(\underline{x}_o))^T u\right)^s\|u\|^{2r}\right)^2}\begin{pmatrix} 2q\left((J\nabla I(\underline{x}_o))^T u\right)\|u\|^2\left(\nabla^2 I(\underline{x})^T\nabla I(\underline{x})\right) \\ +s\|\nabla I(\underline{x})\|^2\|u\|^2 J\nabla I(\underline{x}_o) \\ +2r\|\nabla I(\underline{x})\|^2\left((J\nabla I(\underline{x}_o))^T u\right)u \end{pmatrix}$$

Let $D = \|\nabla I(\underline{x})\|^{2q-2}\left((J\nabla I(\underline{x}_o))^T u\right)^{s-1}\|u\|^{2r-2}$, $E = \left(1+\|\nabla I(\underline{x})\|^{2q}\left((J\nabla I(\underline{x}_o))^T u\right)^s\|u\|^{2r}\right)^2$ and

$G = 2q\left((J\nabla I(\underline{x}_o))^T u\right)\|u\|^2\left(\nabla^2 I(\underline{x})^T\nabla I(\underline{x})\right)+s\|\nabla I(\underline{x})\|^2\|u\|^2 J\nabla I(\underline{x}_o)+2r\|\nabla I(\underline{x})\|^2\left((J\nabla I(\underline{x}_o))^T u\right)u$.

Then ∇F_1 can be re-written as

$$\nabla F_1(\underline{x}) = -\frac{D}{E}G$$

Hence, the Hessian of F_1 is,

$$\nabla^2 F_1(\underline{x}) = -\frac{1}{E}G\nabla(D)^T + \frac{D}{E^2}G\nabla(E)^T - \frac{D}{E}\nabla G$$

Due to minimal point condition in Lemma 5, G=0, then

$$\nabla^2 F_1(\underline{x}) = -\frac{D}{E}\nabla G \qquad (3.19)$$

The gradient ∇G is evaluated to be

$$\nabla G = \begin{pmatrix} 2q\left((J\nabla I(\underline{x}_o))^T u\right)\|u\|^2\nabla\left(\nabla^2 I(\underline{x})^T\nabla I(\underline{x})\right)+4q\left((J\nabla I(\underline{x}_o))^T u\right)\left(\nabla^2 I(\underline{x})^T\nabla I(\underline{x})\right)u^T \\ +2q\|u\|^2\left(\nabla^2 I(\underline{x})^T\nabla I(\underline{x})\right)(J\nabla I(\underline{x}_o))^T \\ +2s\|u\|^2(J\nabla I(\underline{x}_o))\left(\nabla^2 I(\underline{x})^T\nabla I(\underline{x})\right)^T+2s\|\nabla I(\underline{x})\|^2(J\nabla I(\underline{x}_o))u^T \\ +4r\left((J\nabla I(\underline{x}_o))^T u\right)u\left(\nabla^2 I(\underline{x})^T\nabla I(\underline{x})\right)^T+2r\|\nabla I(\underline{x})\|^2 u(J\nabla I(\underline{x}_o))^T \\ +2r\|\nabla I(\underline{x})\|^2\left((J\nabla I(\underline{x}_o))^T u\right)I_{2x2} \end{pmatrix}$$

Substitute the following equation we had obtained from critical point condition in Lemma 5 into ∇G

$$\left(\nabla^2 I(\underline{x})^T \nabla I(\underline{x})\right) = -\frac{s\|\nabla I(\underline{x})\|^2 J\nabla I(\underline{x}_o)}{2q\left((J\nabla I(\underline{x}_o))^T u\right)} - \frac{r\|\nabla I(\underline{x})\|^2 u}{q\|u\|^2}$$

∇G evaluated at a minimal point is:

$$\nabla G = \begin{pmatrix} 2q\left((J\nabla I(\underline{x}_o))^T u\right)\|u\|^2 \nabla\left(\nabla^2 I(\underline{x})^T \nabla I(\underline{x})\right) - 2s\|\nabla I(\underline{x})\|^2 (J\nabla I(\underline{x}_o))u^T \\ -4r\dfrac{\|\nabla I(\underline{x})\|^2\left((J\nabla I(\underline{x}_o))^T u\right)uu^T}{\|u\|^2} - s\dfrac{\|\nabla I(\underline{x})\|^2\|u\|^2 J\nabla I(\underline{x}_o)(J\nabla I(\underline{x}_o))^T}{\left((J\nabla I(\underline{x}_o))^T u\right)} \\ -2r\|\nabla I(\underline{x})\|^2 u(J\nabla I(\underline{x}_o))^T - \dfrac{s^2\|u\|^2\|\nabla I(\underline{x})\|^2 (J\nabla I(\underline{x}_o))(J\nabla I(\underline{x}_o))^T}{q\left((J\nabla I(\underline{x}_o))^T u\right)} \\ -\dfrac{2rs\|\nabla I(\underline{x})\|^2\left((J\nabla I(\underline{x}_o))u^T\right)}{q} + 2s\|\nabla I(\underline{x})\|^2 (J\nabla I(\underline{x}_o))u^T \\ -\dfrac{2rs\|\nabla I(\underline{x})\|^2\left(u(J\nabla I(\underline{x}_o))^T\right)}{q} - \dfrac{4r^2\left((J\nabla I(\underline{x}_o))^T u\right)\|\nabla I(\underline{x})\|^2 uu^T}{q\|u\|^2} \\ +2r\|\nabla I(\underline{x})\|^2 u(J\nabla I(\underline{x}_o))^T + 2r\|\nabla I(\underline{x})\|^2\left((J\nabla I(\underline{x}_o))^T u\right)I_{2x2} \end{pmatrix}$$

Collecting similar terms together,

$$\nabla G = \begin{pmatrix} 2q\left((J\nabla I(\underline{x}_o))^T u\right)\|u\|^2 \nabla\left(\nabla^2 I(\underline{x})^T \nabla I(\underline{x})\right) \\ -4r\left(1+\dfrac{r}{q}\right)\dfrac{\|\nabla I(\underline{x})\|^2\left((J\nabla I(\underline{x}_o))^T u\right)uu^T}{\|u\|^2} \\ -s\left(1+\dfrac{s}{q}\right)\dfrac{\|\nabla I(\underline{x})\|^2\|u\|^2 J\nabla I(\underline{x}_o)(J\nabla I(\underline{x}_o))^T}{\left((J\nabla I(\underline{x}_o))^T u\right)} \\ -\dfrac{2rs\|\nabla I(\underline{x})\|^2\left((J\nabla I(\underline{x}_o))u^T\right)}{q} \\ -\dfrac{2rs\|\nabla I(\underline{x})\|^2\left(u(J\nabla I(\underline{x}_o))^T\right)}{q} \\ +2r\|\nabla I(\underline{x})\|^2\left((J\nabla I(\underline{x}_o))^T u\right)I_{2x2} \end{pmatrix}$$

Substituting ∇G into (3.19), we get the result. □

Proposition 1: For a given point $\underline{x}_o$, there exists a set of positive integeres (q^*, r^*, s^*) such that the real-valued function F_1 admits a non-degenerate local minimum.

Proof: Let q_{d1} be the critical point of F. $\nabla^2 F_1$ at critical point, q_{d1}, is evaluated in Lemma 6. We will deal only with following portion $\nabla^2 F_1(q_{d1})$ since other terms of $\nabla^2 F_1(q_{d1})$ are positive scalar values and have no role in the analysis of positive-definiteness.

$$\begin{pmatrix} -2q\left((J\nabla I(\underline{x}_o))^T u\right)\|u\|^2 \nabla\left(\nabla^2 I(\underline{x})^T \nabla I(\underline{x})\right) \\ +4r\left(1+\frac{r}{q}\right)\frac{\|\nabla I(\underline{x})\|^2\left((J\nabla I(\underline{x}_o))^T u\right)uu^T}{\|u\|^2} \\ +s\left(1+\frac{s}{q}\right)\frac{\|\nabla I(\underline{x})\|^2\|u\|^2 J\nabla I(\underline{x}_o)(J\nabla I(\underline{x}_o))^T}{\left((J\nabla I(\underline{x}_o))^T u\right)} \\ +\frac{2rs\|\nabla I(\underline{x})\|^2\left((J\nabla I(\underline{x}_o))u^T\right)}{q} \\ +\frac{2rs\|\nabla I(\underline{x})\|^2\left(u(J\nabla I(\underline{x}_o))^T\right)}{q} \\ -2r\|\nabla I(\underline{x})\|^2\left((J\nabla I(\underline{x}_o))^T u\right)I_{2x2} \end{pmatrix}$$

In order that q_{d1} is an attractor point, $\nabla^2 F_1(q_{d1})$ should be positive definite and for $\nabla^2 F_1(q_{d1})$ to be positive definite, for any non-zero vector β, $\beta^T\left[\nabla^2 F_1(q_{d1})\right]\beta \geq 0$ should hold.

Choose u and $u^\perp$ be two orthogonal vectors that span the space. It is the case that

$$u^T\left[\nabla^2 F_1(q_{d1})\right]u \geq 0 \qquad \text{and} \qquad \left(u^\perp\right)^T\left[\nabla^2 F_1(q_{d1})\right]\left(u^\perp\right) \geq 0$$

for any β,

$$\beta^T\left[\nabla^2 F_1(q_{d2})\right]\beta \geq 0$$

holds since β can be expressed in terms of u and $u^{\perp}$.

Let's first compute $u^T\left[\nabla^2 F_1(q_{dl})\right]u \geq 0$ and $\left(u^{\perp}\right)^T\left[\nabla^2 F_1(q_{dl})\right]\left(u^{\perp}\right) \geq 0$ and analyze their negative definiteness. $u^T\left[\nabla^2 F_1(q_{dl})\right]u$ is computed in several steps,

$$u^T\left[\nabla^2 F_1(q_{dl})\right]u = u^T\begin{pmatrix} -2q\left((J\nabla I(\underline{x}_o))^T u\right)\|u\|^2\nabla\left(\nabla^2 I(\underline{x})^T\nabla I(\underline{x})\right) \\ +4r\left(1+\frac{r}{q}\right)\frac{\|\nabla I(\underline{x})\|^2\left((J\nabla I(\underline{x}_o))^T u\right)uu^T}{\|u\|^2} \\ +s\left(1+\frac{s}{q}\right)\frac{\|\nabla I(\underline{x})\|^2\|u\|^2 J\nabla I(\underline{x}_o)(J\nabla I(\underline{x}_o))^T}{\left((J\nabla I(\underline{x}_o))^T u\right)} \\ +\frac{2rs\|\nabla I(\underline{x})\|^2\left((J\nabla I(\underline{x}_o))u^T\right)}{q} \\ +\frac{2rs\|\nabla I(\underline{x})\|^2\left(u(J\nabla I(\underline{x}_o))^T\right)}{q} \\ -2r\|\nabla I(\underline{x})\|^2\left((J\nabla I(\underline{x}_o))^T u\right)I_{2x2} \end{pmatrix}u$$

Multiply by u^T and u on the respective sides,

$$u^T\left[\nabla^2 F_1(q_{dl})\right]u = \begin{pmatrix} -2q\left((J\nabla I(\underline{x}_o))^T u\right)\|u\|^2 u^T\nabla\left(\nabla^2 I(\underline{x})^T\nabla I(\underline{x})\right)u \\ +4r\left(1+\frac{r}{q}\right)\frac{\|\nabla I(\underline{x})\|^2\left((J\nabla I(\underline{x}_o))^T u\right)u^T uu^T u}{\|u\|^2} \\ +s\left(1+\frac{s}{q}\right)\frac{\|\nabla I(\underline{x})\|^2\|u\|^2 u^T J\nabla I(\underline{x}_o)(J\nabla I(\underline{x}_o))^T u}{\left((J\nabla I(\underline{x}_o))^T u\right)} \\ +\frac{2rs\|\nabla I(\underline{x})\|^2 u^T\left((J\nabla I(\underline{x}_o))u^T\right)u}{q} \\ +\frac{2rs\|\nabla I(\underline{x})\|^2 u^T\left(u(J\nabla I(\underline{x}_o))^T\right)u}{q} \\ -2r\|\nabla I(\underline{x})\|^2\left((J\nabla I(\underline{x}_o))^T u\right)u^T I_{2x2}u \end{pmatrix}$$

Substitute $u^T u = \|u\|^2$,

$$u^T\left[\nabla^2 F_1(q_{d1})\right]u = \begin{pmatrix} -2q\left((J\nabla I(\underline{x}_o))^T u\right)\|u\|^2 u^T\nabla\left(\nabla^2 I(\underline{x})^T \nabla I(\underline{x})\right)u \\ +4r\left(1+\frac{r}{q}\right)\frac{\|\nabla I(\underline{x})\|^2\left((J\nabla I(\underline{x}_o))^T u\right)\|u\|^4}{\|u\|^2} \\ +s\left(1+\frac{s}{q}\right)\|\nabla I(\underline{x})\|^2\|u\|^2 u^T J\nabla I(\underline{x}_o) \\ +\frac{2rs\|\nabla I(\underline{x})\|^2\left(u^T(J\nabla I(\underline{x}_o))\right)\|u\|^2}{q} \\ +\frac{2rs\|\nabla I(\underline{x})\|^2\|u\|^2\left((J\nabla I(\underline{x}_o))^T u\right)}{q} \\ -2r\|\nabla I(\underline{x})\|^2\left((J\nabla I(\underline{x}_o))^T u\right)\|u\|^2 \end{pmatrix}$$

Simplify the expression by canncelling out similar terms,

$$u^T\left[\nabla^2 F_1(q_{d1})\right]u = \begin{pmatrix} -2q\left((J\nabla I(\underline{x}_o))^T u\right)\|u\|^2 u^T\nabla\left(\nabla^2 I(\underline{x})^T \nabla I(\underline{x})\right)u \\ +4r\left(1+\frac{r}{q}\right)\|\nabla I(\underline{x})\|^2\left((J\nabla I(\underline{x}_o))^T u\right)\|u\|^2 \\ +s\left(1+\frac{s}{q}\right)\|\nabla I(\underline{x})\|^2\|u\|^2 u^T J\nabla I(\underline{x}_o) \\ +\frac{2rs\|\nabla I(\underline{x})\|^2\left(u^T(J\nabla I(\underline{x}_o))\right)\|u\|^2}{q} \\ +\frac{2rs\|\nabla I(\underline{x})\|^2\|u\|^2\left((J\nabla I(\underline{x}_o))^T u\right)}{q} \\ -2r\|\nabla I(\underline{x})\|^2\left((J\nabla I(\underline{x}_o))^T u\right)\|u\|^2 \end{pmatrix}$$

Common terms are taken out,

$$u^T\left[\nabla^2 F_1(q_{d1})\right]u = \|u\|^2\left((J\nabla I(\underline{x}_o))^T u\right)\begin{pmatrix} -2qu^T\nabla\left(\nabla^2 I(\underline{x})^T \nabla I(\underline{x})\right)u \\ +\left(2r\left(1+\frac{2r}{q}\right)+s\left(1+\frac{s}{q}\right)+\frac{4rs}{q}\right)\|\nabla I(\underline{x})\|^2 \end{pmatrix} \qquad (3.20)$$

For the right of (3.20) to be greater than zero,

$$\left((J\nabla I(\underline{x}_o))^T u\right)2qu^T\nabla\left(\nabla^2 I(\underline{x})^T \nabla I(\underline{x})\right)u \le (2r+s)\left(\frac{2r+s+q}{q}\right)\left\|\nabla I(\underline{x})\right\|^2\left((J\nabla I(\underline{x}_o))^T u\right) \tag{3.21}$$

should hold. Define θ to be the angle between u and $(J\nabla I(\underline{x}_o))$. Then

$$(J\nabla I(\underline{x}_o))^T u = \left\|J\nabla I(\underline{x}_o)\right\|\left\|u\right\|\text{Cos}\theta$$

Substituting in (3.21),

$$2\left\|J\nabla I(\underline{x}_o)\right\|\left\|u\right\|\text{Cos}\theta qu^T\nabla\left(\nabla^2 I(\underline{x})^T \nabla I(\underline{x})\right)u \le (2r+s)\left(\frac{2r+s+q}{q}\right)\left\|\nabla I(\underline{x})\right\|^2\left\|J\nabla I(\underline{x}_o)\right\|\left\|u\right\|\text{Cos}\theta$$

Eliminating similar terms on both sides of the inequality,

$$\text{Cos}\theta u^T\nabla\left(\nabla^2 I(\underline{x})^T \nabla I(\underline{x})\right)u \le (2r+s)\left(\frac{2r+s+q}{2q^2}\right)\left\|\nabla I(\underline{x})\right\|^2\text{Cos}\theta \tag{3.22}$$

$\text{Cos}\theta > 0$ so that the angle between u and $(J\nabla I(\underline{x}_o))$ is less than $\pi/2$, that is u and $(J\nabla I(\underline{x}_o))$ have similar directions. If $\text{Cos}\theta > 0$, then for $u^T\left[\nabla^2 F_l(q_{dl})\right]u \ge 0$, the following should hold.

$$\frac{u^T\nabla\left(\nabla^2 I(\underline{x})^T \nabla I(\underline{x})\right)u}{\left\|\nabla I(\underline{x})\right\|^2} \le (2r+s)\left(\frac{2r+s+q}{2q^2}\right) \tag{3.23}$$

Now, let us determine $u^{\perp T}\nabla^2 F_l(q_{dl})u^{\perp}$

$$u^{\perp T}\nabla^2 F_l(q_{dl})u^{\perp} = \begin{pmatrix} -2q\left((J\nabla I(\underline{x}_o))^T u\right)\|u\|^2 u^{\perp T}\nabla\left(\nabla^2 I(\underline{x})^T \nabla I(\underline{x})\right)u^{\perp} \\ +4r\left(1+\frac{r}{q}\right)\frac{\|\nabla I(\underline{x})\|^2\left((J\nabla I(\underline{x}_o))^T u\right)u^{\perp T}uu^T u^{\perp}}{\|u\|^2} \\ +s\left(1+\frac{s}{q}\right)\frac{\|\nabla I(\underline{x})\|^2\|u\|^2 u^{\perp T}J\nabla I(\underline{x}_o)(J\nabla I(\underline{x}_o))^T u^{\perp}}{\left((J\nabla I(\underline{x}_o))^T u\right)} \\ +\frac{2rs\|\nabla I(\underline{x})\|^2 u^{\perp T}\left((J\nabla I(\underline{x}_o))u^T\right)u^{\perp}}{q} \\ +\frac{2rs\|\nabla I(\underline{x})\|^2 u^{\perp T}\left(u(J\nabla I(\underline{x}_o))^T\right)u^{\perp}}{q} \\ -2r\|\nabla I(\underline{x})\|^2\left((J\nabla I(\underline{x}_o))^T u\right)u^{\perp T}I_{2x2}u^{\perp} \end{pmatrix}$$

Some terms turn out to be zero due to the fact that $u^{\perp T}u = 0$,

$$u^{\perp T}\nabla^2 F_l(q_{dl})u^{\perp} = \begin{pmatrix} -2q\left((J\nabla I(\underline{x}_o))^T u\right)\|u\|^2 u^{\perp T}\nabla\left(\nabla^2 I(\underline{x})^T \nabla I(\underline{x})\right)u^{\perp} \\ +s\left(1+\frac{s}{q}\right)\frac{\|\nabla I(\underline{x})\|^2\|u\|^2 u^{\perp T}J\nabla I(\underline{x}_o)(J\nabla I(\underline{x}_o))^T u^{\perp}}{\left((J\nabla I(\underline{x}_o))^T u\right)} \\ -2r\|\nabla I(\underline{x})\|^2\left((J\nabla I(\underline{x}_o))^T u\right)\|u^{\perp}\|^2 \end{pmatrix}$$

Common terms are taken out,

$$u^{\perp T}\nabla^2 F_l(q_{dl})u^{\perp} = \|u\|^2\begin{pmatrix} -2q\left((J\nabla I(\underline{x}_o))^T u\right)u^{\perp T}\nabla\left(\nabla^2 I(\underline{x})^T \nabla I(\underline{x})\right)u^{\perp} \\ +s\left(1+\frac{s}{q}\right)\frac{\|\nabla I(\underline{x})\|^2 u^{\perp T}J\nabla I(\underline{x}_o)(J\nabla I(\underline{x}_o))^T u^{\perp}}{\left((J\nabla I(\underline{x}_o))^T u\right)} \\ -2r\|\nabla I(\underline{x})\|^2\left((J\nabla I(\underline{x}_o))^T u\right) \end{pmatrix}$$

Again, define θ to be the angle between u and $(J\nabla I(\underline{x}_o))$. Then the angle between $u^{\perp}$ and $(J\nabla I(\underline{x}_o))$ is $\pi/2 - \theta$. Using this fact, $u^{\perp T}\nabla^2 F_l(q_{dl})u^{\perp}$ becomes

$$u^{\perp T}\nabla^2 F_1(q_{d1})u^{\perp} = \|u\|^2 \begin{pmatrix} -2q\|J\nabla I(\underline{x}_o)\|\|u\|\mathrm{Cos}\theta U^{\perp T}\nabla\left(\nabla^2 I(\underline{x})^T \nabla I(\underline{x})\right)u^{\perp} \\ +s\left(1+\frac{s}{q}\right)\frac{\|\nabla I(\underline{x})\|^2 \|J\nabla I(\underline{x}_o)\|\|u\|\mathrm{Sin}\theta\|J\nabla I(\underline{x}_o)\|\|u\|\mathrm{Sin}\theta}{\|J\nabla I(\underline{x}_o)\|\|u\|\mathrm{Cos}\theta} \\ -2r\|\nabla I(\underline{x})\|^2\|J\nabla I(\underline{x}_o)\|\|u\|\mathrm{Cos}\theta \end{pmatrix}$$

Simplifying,

$$u^{\perp T}\nabla^2 F_1(q_{d1})u^{\perp} = \|u\|^2\|J\nabla I(\underline{x}_o)\|\|u\|\begin{pmatrix} -2q\mathrm{Cos}\theta u^{\perp T}\nabla\left(\nabla^2 I(\underline{x})^T\nabla I(\underline{x})\right)u^{\perp} \\ +\left(s\left(1+\frac{s}{q}\right)\frac{\mathrm{Sin}^2\theta}{\mathrm{Cos}\theta}-2r\mathrm{Cos}\theta\right)\|\nabla I(\underline{x})\|^2 \end{pmatrix}$$

$$\mathrm{Cos}\theta u^{\perp T}\nabla\left(\nabla^2 I(\underline{x})^T\nabla I(\underline{x})\right)u^{\perp} \le \frac{1}{2q}\left(s\left(1+\frac{s}{q}\right)\frac{\mathrm{Sin}^2\theta}{\mathrm{Cos}\theta}-2r\mathrm{Cos}\theta\right)\|\nabla I(\underline{x})\|^2$$

$$\mathrm{Cos}\theta\frac{u^{\perp T}\nabla\left(\nabla^2 I(\underline{x})^T\nabla I(\underline{x})\right)u^{\perp}}{\|\nabla I(\underline{x})\|^2} \le \frac{1}{2q}\left(s\left(1+\frac{s}{q}\right)\frac{\mathrm{Sin}^2\theta}{\mathrm{Cos}\theta}-2r\mathrm{Cos}\theta\right) \qquad (3.24)$$

These results indicate that q, r and s values can be computed, so that these inequalities (3.22) and (3.24) hold. Thus, choosing appropriate q, r and s values, positive defineteness of F_1 around minimal point can be achieved. □

3.3. Tracing Based on Fixation Points

The aim of this stage is use the fixation points thus generated in a specific task - namely the tracing of an object's outline.

First let γ_2 represent a potential well centered at the points $\underline{x}$ at which the Euclidean distance from the next fixation point x^{k+1} is minimal as:

$$\gamma_2(\underline{x}, x^{k+1}) = \left(\underline{x} - x^{k+1}\right)^T\left(\underline{x} - x^{k+1}\right) \qquad (3.25)$$

Next, obstacle points are enclosed by just one term - a β_2 term that marks those points where the image gradient vanishes as obstacles as:

$$\beta_2(\underline{x}) = \nabla I(\underline{x})^T \nabla I(\underline{x}) \tag{3.26}$$

The obstacle space O_2 is defined

$$O_2 = \{\underline{x} \in C : \beta_2(\underline{x}) \le 0\} \tag{3.27}$$

Constructed in a manner similar to [34,35], the artificial potential function is a two parameter family defined by the composition of three functions:

$$F_2(\underline{x}, x^{k+1}) = \sigma_d \circ \sigma \circ \varphi_{2mn}(\underline{x}, x^{k+1}) \tag{3.28}$$

where the function φ_{2mn} is defined as:

$$\varphi_{2mn} = \frac{\gamma_2^m}{\beta_2^n}, \tag{3.29}$$

the squashing function σ is defined in (3.8) and the sharpening function σ_d is defined by

$$\sigma_d(y) = y^Q \tag{3.30}$$

where Q=max(m,n). The parameters m and n are used to control the shape of the φ_{2mn}. Since φ_{2mn} blows up at some points, to correct this undesired behaviour, the image of φ_{2mn} is squashed by the map $\sigma : [0,\infty) \to [0,1]$. This function is defined over all the domain and is also admissible. Finally due to parameter Q, the destination point x^{k+1} is degenerate critical point. To counteract this effect, the sharpening function $\sigma_d : [0,1] \to [0,1]$ is introduced to change the x^{k+1} to a degenerate critical point. Note that the first derivative of both functions are strictly positive for x>0. Therefore, the surface properties of φ_{2mn} are

invariant under these maps. By construction, the case $\dot{x} = 0$ can happen only at x^{k+1} and if φ_{2mn} has a nondegenerate minimum at this point.

Here, all functions γ_2, φ_{2mn} and F_2 are dependent on x^{k+1} but for the simplification of the notation, the second argument x^{k+1} will be omitted in the sequel .

The initial condition is x^k. The following proposition establishes that the next fixation point x^{k+1} is an attracting critical point of F_2.

Proposition: For a finite m, the point x^{k+1} is a stable critical point of the artificial potential function F_2 .

3.3.1. Theoretical Anaysis of Tracing Object's Outline

Recall:

$$\varphi_{2mn}(\underline{x}) = \frac{(v^T v)^m}{(\nabla I(\underline{x})^T \nabla I(\underline{x}) + 1)^n} \tag{3.31}$$

Here, $\underline{x}$ is the candidate for next point to be generated. $I(\underline{x})$ is the intensity at $\underline{x}$. $\nabla I(\underline{x})$ is the gradient of I at $\underline{x}$,

$$\nabla I(\underline{x}) = \begin{bmatrix} I_x(\underline{x}) \\ I_y(\underline{x}) \end{bmatrix} \tag{3.32}$$

v is the vector between $\underline{x}$ and $\underline{x}_f$,

$$v = \underline{x}_f - \underline{x} = \begin{bmatrix} x_f - x \\ y_f - y \end{bmatrix} \tag{3.33}$$

where $\underline{x}_f$ is the target point x^{k+1}.

Through composition (3.28), F_2 is

$$F_2(\underline{x}) = \frac{\left(v^T v\right)}{\left(\left(v^T v\right)^m + \left(\nabla I(\underline{x})^T \nabla I(\underline{x}) + 1\right)^n\right)^{1/m}} \tag{3.34}$$

The following technical lemmas give the formulas for the gradient and the Hessian (second derivative) of F_2 which will be used continually in the sequel.

Lemma 1: The gradient F_2 is

$$\nabla F_2(\underline{x}) = \frac{-2\left(\|\nabla I(\underline{x})\|^2 + 1\right)^n \left(v + \frac{n\|v\|^2 \left(\nabla^2 I(\underline{x})^T \nabla I(\underline{x})\right)}{m\left(\|\nabla I(\underline{x})\|^2 + 1\right)}\right)}{\left(\|v\|^{2m} + \left(\|\nabla I(\underline{x})\|^2 + 1\right)^n\right)^{1/m+1}} \tag{3.35}$$

Proof: For the sake of simplicity, let $A = v^T v$ and $B = \left(\nabla I(\underline{x})^T \nabla I(\underline{x}) + 1\right)^n$. Then $\nabla A = 2v$ and $\nabla B = -2m\left(v^T v\right)^{m-1} v + 2n\left(\nabla I^T \nabla I + 1\right)^{n-1}\left(\nabla^2 I^T \nabla I\right)$ and F_2 is,

$$F_2(\underline{x}) = \frac{A}{(B)^{1/m}}$$

$$\nabla F_2 = \frac{1}{(B)^{1/m}} \nabla A - \frac{A}{m(B)^{1/m+1}} \nabla B$$

Let's substitute A, B, ∇A and ∇B back into ∇F_2,

$$\nabla F_2(\underline{x}) = \frac{-2v}{\left(\|v\|^{2m} + \left(\|\nabla I\|^2 + 1\right)^n\right)^{1/m}} - \frac{\left(v^T v\right)\left(-2m\|v\|^{2m-2} v + 2n\left(\|\nabla I\|^2 + 1\right)^{n-1}\left(\nabla^2 I^T \nabla I\right)\right)}{m\left(\|v\|^{2m} + \left(\|\nabla I\|^2 + 1\right)^n\right)^{1/m+1}}$$

Simplifying, we get

$$\nabla F_2(\underline{x}) = \frac{-2\left(\|\nabla I\|^2 + 1\right)^n \left(v + \frac{n\|v\|^2 \left(\nabla^2 I^T \nabla I\right)}{m\left(\|\nabla I\|^2 + 1\right)} \right)}{\left(\|v\|^{2m} + \left(\|\nabla I\|^2 + 1\right)^n \right)^{1/m+1}}$$

Hence, we get the stated result. □

The following lemma establishes the critical points of F_2.

Lemma 2: At critical points of F_2, following must hold:

$$v + \frac{n\|v\|^2 \left(\nabla^2 I^T \nabla I\right)}{m\left(\|\nabla I\|^2 + 1\right)} = 0 \tag{3.36}$$

Proof: Critical points are obtained by equalizing the gradient $\nabla F_2=0$. From Lemma 1, we see that ∇F_2 is equal to zero either when

$$v=0 \qquad \text{or} \qquad v + \frac{n\|v\|^2 \left(\nabla^2 I^T \nabla I\right)}{m\left(\|\nabla I\|^2 + 1\right)} = 0 \quad . \square$$

Lemma 3: The Hessian of F_2 evaluated at minimal points is

$$\nabla^2 F_2(\underline{x}) = \frac{2\left(\|\nabla I\|^2 + 1\right)^n \left(I_{2x2} + \frac{2n\left(\nabla^2 I^T \nabla I\right) v^T}{m\left(\|\nabla I\|^2 + 1\right)} - \frac{n\|v\|^2 \nabla\left(\nabla^2 I^T \nabla I\right)}{m\left(\|\nabla I\|^2 + 1\right)} + \frac{2n\|v\|^2 \left(\nabla^2 I^T \nabla I\right)\left(\nabla^2 I^T \nabla I\right)^T}{m\left(\|\nabla I\|^2 + 1\right)} \right)}{\left(\|v\|^{2m} + \left(\|\nabla I\|^2 + 1\right)^n \right)^{1/m+1}} \tag{3.37}$$

Proof: For the sake of simplicity, let

$$D = \left(\|\nabla I\|^2 + 1\right)^n, \qquad E = \left(\|v\|^{2m} + \left(\|\nabla I\|^2 + 1\right)^n \right)^{1/m+1} \qquad \text{and} \qquad C = v + \frac{n\|v\|^2 \left(\nabla^2 I^T \nabla I\right)}{m\left(\|\nabla I\|^2 + 1\right)}$$

Then

$$\nabla F_2 = \frac{-2D}{E} C \tag{3.38}$$

Differentiating ∇F_2, $\nabla^2 F_2$ is found to be

$$\nabla^2 F_2 = -2\left(\frac{1}{E} C(\nabla D)^T - \frac{D}{E^2} C(\nabla E)^T + \frac{D}{E}(\nabla C)\right)$$

Evaluated at a critical point, C=0 as proved in Lemma 2. Thus, $\nabla^2 F_2$ reduces to

$$\nabla^2 F_2 = -2\left(\frac{D}{E}(\nabla C)\right)$$

Differentiating C, ∇C is found to be,

$$\nabla C = -I_{2x2} - \frac{2n\left(\nabla^2 I^T \nabla I\right)}{m\left(\|\nabla I\|^2 + 1\right)} v^T + \frac{n\|v\|^2}{m\left(\|\nabla I\|^2 + 1\right)} \nabla\left(\nabla^2 I^T \nabla I\right) - \frac{2n\|v\|^2}{m\left(\|\nabla I\|^2 + 1\right)} \left(\nabla^2 I^T \nabla I\right)\left(\nabla^2 I^T \nabla I\right)^T$$

Substituting for C, D and E in equation (3.38), we get

$$\nabla^2 F_2(\underline{x}) = \frac{2\left(\|\nabla I\|^2 + 1\right)^n \left(I_{2x2} + \frac{2n\left(\nabla^2 I^T \nabla I\right) v^T}{m\left(\|\nabla I\|^2 + 1\right)} - \frac{n\|v\|^2 \nabla\left(\nabla^2 I^T \nabla I\right)}{m\left(\|\nabla I\|^2 + 1\right)} + \frac{2n\|v\|^2 \left(\nabla^2 I^T \nabla I\right)\left(\nabla^2 I^T \nabla I\right)^T}{m\left(\|\nabla I\|^2 + 1\right)} \right)}{\left(\|v\|^{2m} + \left(\|\nabla I\|^2 + 1\right)^n \right)^{1/m+1}}$$

We see that the point $x=x^{k+1}$ is a critical point of F_2 since v=0 which then implies that $\nabla F_2=0$. □

First we shall see that x^{k+1} is a non-degenerate local minimum.

Proposition 1: The point x^{k+1} is a non-degenerate local minimum of F_2.

Proof: Note that at x^{k+1}, v=0. The Hessian $\nabla^2 F_2$ evaluated at x^{k+1} is

$$\nabla^2 F_2\left(x^{k+1}\right)=\frac{2\left(\|\nabla I\|^2+1\right)^n I_{2x2}}{\left(\left(\|\nabla I\|^2+1\right)^n\right)^{1/m+1}} \tag{3.39}$$

Because determinant of $\nabla^2 F_2\left(x^{k+1}\right)$ is always positive, x^{k+1} is a non-degenerate local minimum. □

3.3.1.1. <u>The Absence of Undesired Local Minima:</u> We also observe that F_2 has critical points also at points where

$$v+\frac{n\|v\|^2\left(\nabla^2 I^T \nabla I\right)}{m\left(\|\nabla I\|^2+1\right)}=0$$

holds, but v≠0. It turns out that we can choose the parameters m and n such that all critical points of F_2 other than x^{k+1} are saddles. This idea is made precise in Proposition 2. The proof that follows has two steps: First, a lemma shows the form of the Hessian at all critical points other than x^{k+1}. Then, a test direction along which the Hessian has a negative eigenvalue is found. As a result, excepting the minimum at x^{k+1}, all the other critical points are not local minimum. In this case, for all initial points except for a set of measure zero, the gradient system will end up at x^{k+1}.

The following Lemma gives the formula for Hessian evaluated at critical points other than x^{k+1}.

Lemma 4: Hessian of F_2 evaluated at a critical point other than x^{k+1} is

$$\nabla^2 F_2(\underline{x})=\frac{2\left(\|\nabla I\|^2+1\right)^n\left(I_{2x2}+2\left(\frac{m}{n}-1\right)\frac{vv^T}{v^T v}-\frac{n\|v\|^2\nabla\left(\nabla^2 I^T\nabla I\right)}{m\left(\|\nabla I\|^2+1\right)}\right)}{\left(\|v\|^{2m}+\left(\|\nabla I\|^2+1\right)^n\right)^{1/m+1}} \tag{3.40}$$

Proof: Let $q_{d2} \neq x^{k+1}$ be any other critical point point of F_2. $\nabla^2 F_2$ is computed in Lemma 3. Substituting (3.36) into $\nabla^2 F_2$, $\nabla^2 F_2(q_{d2})$ simplies to be,

$$\nabla^2 F_2(q_{d2}) = \frac{2\left(\|\nabla I\|^2 + 1\right)^n \left(I_{2x2} + 2\left(\frac{m}{n} - 1\right)\frac{vv^T}{v^T v} - \frac{n\|v\|^2 \nabla\left(\nabla^2 I^T \nabla I\right)}{m\left(\|\nabla I\|^2 + 1\right)} \right)}{\left(\|v\|^{2m} + \left(\|\nabla I\|^2 + 1\right)^n \right)^{1/m+1}}$$

. □

Proposition 2: For a given point x^{k+1}, there exists a set of integers (m, n) such that there are no minimal points of F_2 other than x^{k+1}.

Proof: Let $q_{d2} \neq x^{k+1}$ be any other critical point point of F_2. If q_{d2} is not a minimal point, then it should be the case that there exists a direction β such that $\beta^T \left[\nabla^2 F_2(q_{d2})\right]\beta < 0$. In the sequel, we show that for carefully chosen (m,n) set, such a test direction can be found.

Let v and $v^{\perp}$ be two orthogonal vectors that span the space. If, it is the case that

$$v^T \left[\nabla^2 F_2(q_{d2})\right] v < 0 \quad \text{and} \quad \left(v^{\perp}\right)^T \left[\nabla^2 F_2(q_{d2})\right]\left(v^{\perp}\right) < 0$$

then

$$\beta^T \left[\nabla^2 F_2(q_{d2})\right]\beta < 0$$

holds since β can be expressed in terms of v and $v^{\perp}$.

Let's first compute $v^T \left[\nabla^2 F_2(q_{d2})\right] v$ and $\left(v^{\perp}\right)^T \left[\nabla^2 F_2(q_{d2})\right]\left(v^{\perp}\right)$ and analyze their negative definiteness. $v^T \left[\nabla^2 F_2(q_{d2})\right] v$ is computed in several steps,

$$v^T \left[\nabla^2 F_2(q_{d2})\right] v = \frac{2\left(\|\nabla I\|^2 + 1\right)^n}{\left(\|v\|^{2m} + \left(\|\nabla I\|^2 + 1\right)^n \right)^{1/m+1}} v^T \left(I_{2x2} + 2\left(\frac{m}{n} - 1\right)\frac{vv^T}{v^T v} - \frac{n\|v\|^2 \nabla\left(\nabla^2 I^T \nabla I\right)}{m\left(\|\nabla I\|^2 + 1\right)} \right) v$$

$$v^T\left[\nabla^2 F_2(q_{d2})\right]v = \frac{2\left(\left\|\nabla I\right\|^2+1\right)^n}{\left(\left\|v\right\|^{2m}+\left(\left\|\nabla I\right\|^2+1\right)^n\right)^{1/m+1}}\left(\left\|v\right\|^2+2\left(\frac{m}{n}-1\right)\frac{\left\|v\right\|^4}{\left\|v\right\|^2}-\frac{n\left\|v\right\|^2 v^T\left[\nabla\left(\nabla^2 I^T\nabla I\right)\right]v}{m\left(\left\|\nabla I\right\|^2+1\right)}\right)$$

$$v^T\left[\nabla^2 F_2(q_{d2})\right]v = \frac{2\left(\left\|\nabla I\right\|^2+1\right)^n\left\|v\right\|^2}{\left(\left\|v\right\|^{2m}+\left(\left\|\nabla I\right\|^2+1\right)^n\right)^{1/m+1}}\left(1+2\left(\frac{m}{n}-1\right)-\frac{nv^T\left[\nabla\left(\nabla^2 I^T\nabla I\right)\right]v}{m\left(\left\|\nabla I\right\|^2+1\right)}\right)$$

Since

$$\frac{2\left(\left\|\nabla I\right\|^2+1\right)^n\left\|v\right\|^2}{\left(\left\|v\right\|^{2m}+\left(\left\|\nabla I\right\|^2+1\right)^n\right)^{1/m+1}}$$

is a positive scalar value, we ignore it, and analyze only

$$\left(1+2\left(\frac{m}{n}-1\right)-\frac{nv^T\left[\nabla\left(\nabla^2 I^T\nabla I\right)\right]v}{m\left(\left\|\nabla I\right\|^2+1\right)}\right)<0$$

Finally, we obtain following inequality

$$\frac{v^T\left[\nabla\left(\nabla^2 I^T\nabla I\right)\right]v}{\left(\left\|\nabla I\right\|^2+1\right)}>\frac{m}{n}\left(2\frac{m}{n}-1\right) \tag{3.41}$$

Similarly $\left(v^\perp\right)^T\left[\nabla^2 F(q_{d2})\right]\left(v^\perp\right)$ is computed in following steps,

$$\left(v^\perp\right)^T\left[\nabla^2 F(q_{d2})\right]\left(v^\perp\right)=\frac{2\left(\left\|\nabla I\right\|^2+1\right)^n\left(v^\perp\right)^T\left(I_{2x2}+2\left(\frac{m}{n}-1\right)\frac{vv^T}{v^Tv}-\frac{n\left\|v\right\|^2\nabla\left(\nabla^2 I^T\nabla I\right)}{m\left(\left\|\nabla I\right\|^2+1\right)}\right)\left(v^\perp\right)}{\left(\left\|v\right\|^{2m}+\left(\left\|\nabla I\right\|^2+1\right)^n\right)^{1/m+1}}$$

$$\left(v^\perp\right)^T\left[\nabla^2 F(q_{d2})\right]\left(v^\perp\right)=\frac{2\left(\left\|\nabla I\right\|^2+1\right)^n}{\left(\left\|v\right\|^{2m}+\left(\left\|\nabla I\right\|^2+1\right)^n\right)^{1/m+1}}\left(\left\|v^\perp\right\|^2+0-\frac{n\left\|v\right\|^2\left(v^\perp\right)^T\nabla\left(\nabla^2 I^T\nabla I\right)\left(v^\perp\right)}{m\left(\left\|\nabla I\right\|^2+1\right)}\right)$$

Here again, we will analyze only

$$\left(\left\| v^{\perp} \right\|^2 - \frac{n\|v\|^2 \left(v^{\perp}\right)^T \nabla\left(\nabla^2 I^T \nabla I\right)\left(v^{\perp}\right)}{m\left(\|\nabla I\|^2 + 1\right)} \right) < 0$$

Because $\left\| v^{\perp} \right\|^2 = \|v\|^2$, finally, we obtain following inequality

$$\frac{\left(v^{\perp}\right)^T \nabla\left(\nabla^2 I^T \nabla I\right)\left(v^{\perp}\right)}{\left(\|\nabla I\|^2 + 1\right)} > \frac{m}{n} \qquad (3.42)$$

If λ_1 and λ_2 are eigenvalues of $\nabla\left(\nabla^2 I^T \nabla I\right)$ and v=[a , b]^T, then

$$\left(v^{\perp}\right)^T \nabla\left(\nabla^2 I^T \nabla I\right)\left(v^{\perp}\right) = \begin{bmatrix} -b & a \end{bmatrix} \begin{bmatrix} \lambda_1 & 0 \\ 0 & \lambda_2 \end{bmatrix} \begin{bmatrix} -b \\ a \end{bmatrix} = b^2\lambda_1 + a^2\lambda_2$$

$$v^T \nabla\left(\nabla^2 I^T \nabla I\right) v = \begin{bmatrix} a & b \end{bmatrix} \begin{bmatrix} \lambda_1 & 0 \\ 0 & \lambda_2 \end{bmatrix} \begin{bmatrix} a \\ b \end{bmatrix} = a^2\lambda_1 + b^2\lambda_2$$

For q_{d2} not to be an attractor point –local minima-, n and m parameters should be chosen such that both

$$\frac{v^T\left[\nabla\left(\nabla^2 I^T \nabla I\right)\right]v}{\left(\|\nabla I\|^2 + 1\right)} > \frac{m}{n}\left(2\frac{m}{n} - 1\right) \qquad \text{and} \qquad \frac{\left(v^{\perp}\right)^T \nabla\left(\nabla^2 I^T \nabla I\right)\left(v^{\perp}\right)}{\left(\|\nabla I\|^2 + 1\right)} > \frac{m}{n}$$

are satisfied.

Or equivalently, if λ_1 and λ_2 are eigenvalues of $\nabla\left(\nabla^2 I^T \nabla I\right)$ and v=[a , b]^T, following inequalities should hold,

$$\frac{a^2\lambda_1 + b^2\lambda_2}{\left(\|\nabla I\|^2 + 1\right)} > \frac{m}{n}\left(2\frac{m}{n} - 1\right) \qquad \text{and} \qquad \frac{b^2\lambda_1 + a^2\lambda_2}{\left(\|\nabla I\|^2 + 1\right)} > \frac{m}{n}$$

. □

4. EXPERIMENTS

We implemented the presented mathematical framework within the visual system of the BUVIS- a visual inspection station developed within our laboratory. The system components are shown in Figure 4.1. Visual processing is done on the Smarteye Vision System which is designed around a high performance DSP chip TMS320C31PQL [47]. Computationally intensive parts of the program are directly programmed in TI assembly language. The remaining parts are programmed in C and then cross-compiled to TI assembly code. The illumination system consists of four lamps located so as to minimize the shadowing effects of each lamp. To-be-inspected parts are placed on an assembly line at an *arbitrary* position and orientation. A camera located exactly above the assembly line views the objects orthographically. An image of the 'to-be-inspected' part is taken and is subjected to further processing in order to determine whether it has any deviations from its CAD specs.

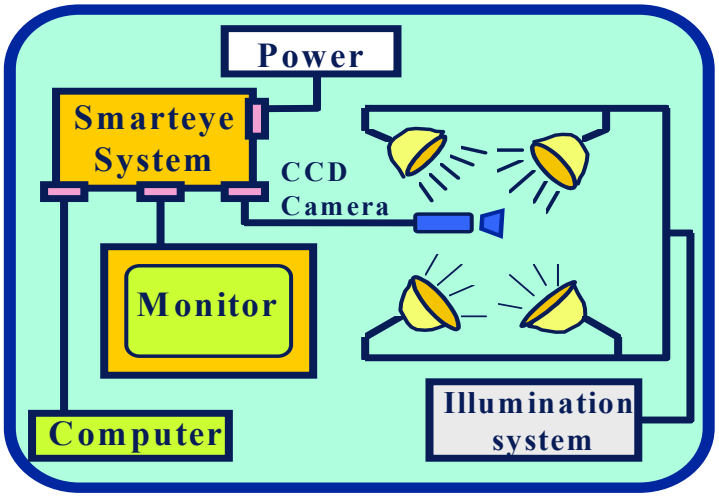

FIGURE 4.1 System Components.

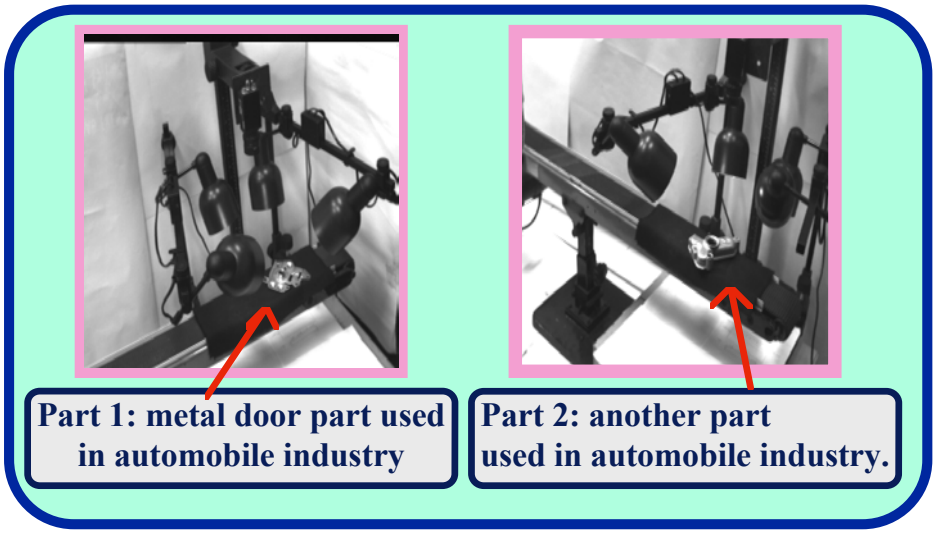

FIGURE 4.2 Inspection of various parts.

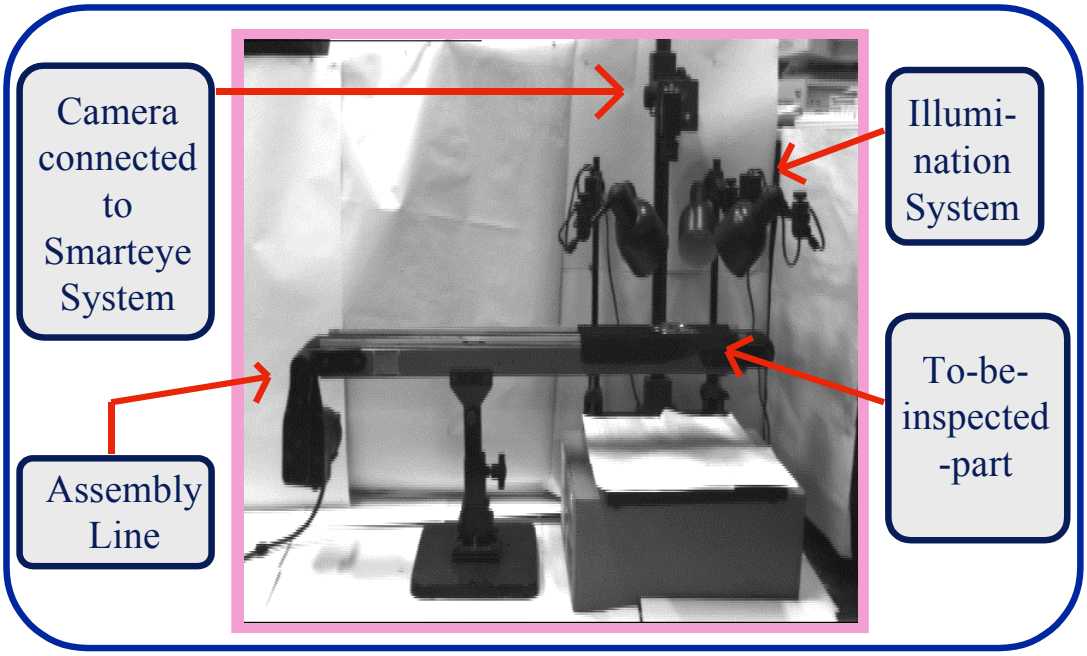

FIGURE 4.3 Experimental Setup of BUVIS.

Two set of experiments were held. In the first set, we demonstrate samples from the processing on a simple odd-shaped object. In the second set, the performance of the proposed approach on industrial objects under varying lighting conditions is presented.

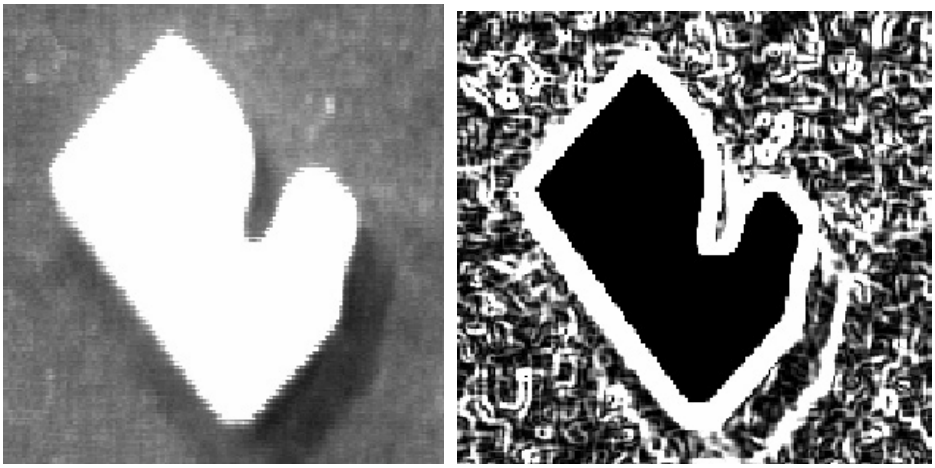

FIGURE 4.4 (a) Odd-shaped object (b) after sharpening.

4.1. Sampled Stages of Processing

In these experiments, an odd-shaped object shown in Figure 4.4(a) is used. Note that the image is a very noisy one with shadows - as seen in Figure 4.4(b) after sharpening operation.

4.1.1. Generation of Fixation Points

Through Figures 4.5-4.7, the generation of the first few fixation points on our odd-shaped object and potential field surfaces around these fixation points are shown. In leftmost figures, the paths leading to next fixation point are generated. The values of q, r, and s are 0.5, 1.6, and 1.5 respectively. In rightmost figures, a cross-section of $F_1(x; x^k)$ surface- for the given potential field around x^k - is shown. The white squares in images are

fixation points. Note that the next fixation point, x^{k+1} occurs in the dark region as minima of $F_1(x; x^k)$ as expected. E.g. local minima of $F_1(x; x^1)$ surface in Figure 4.5(b) indicates location of 2^{nd} fixation point in Figure 4.5(a).

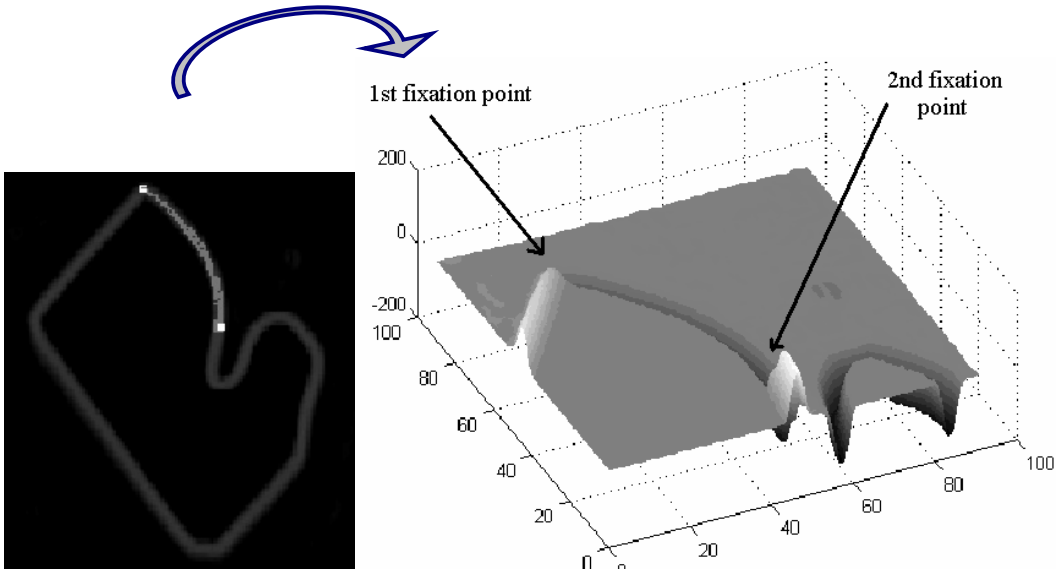

FIGURE 4.5 (a) Path leading to 2^{nd} fix. pt. (b) $F_1(x; x^1)$ surface.

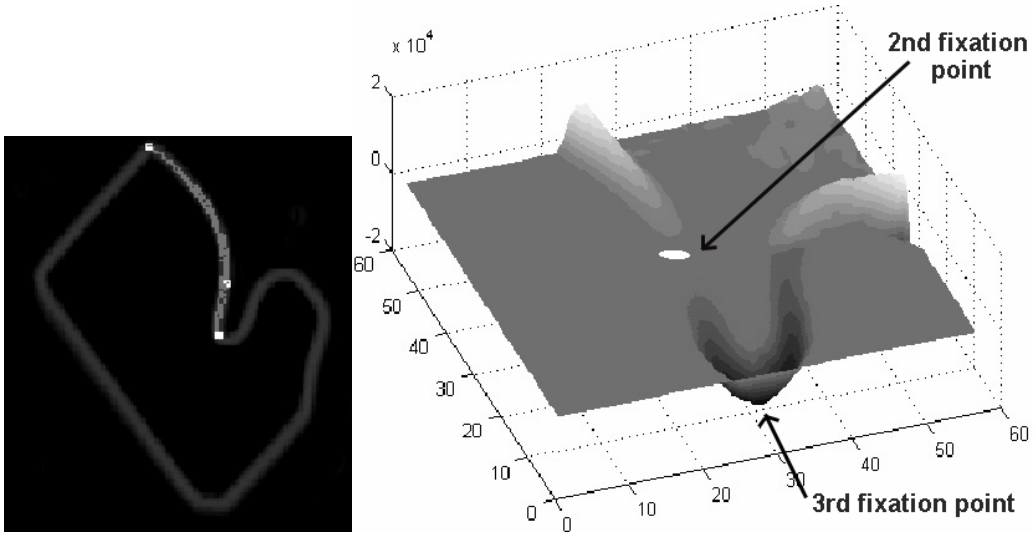

FIGURE 4.6 (a) Path leading to 3^{rd} fix. pt. (b) $F_1(x; x^2)$ surface.

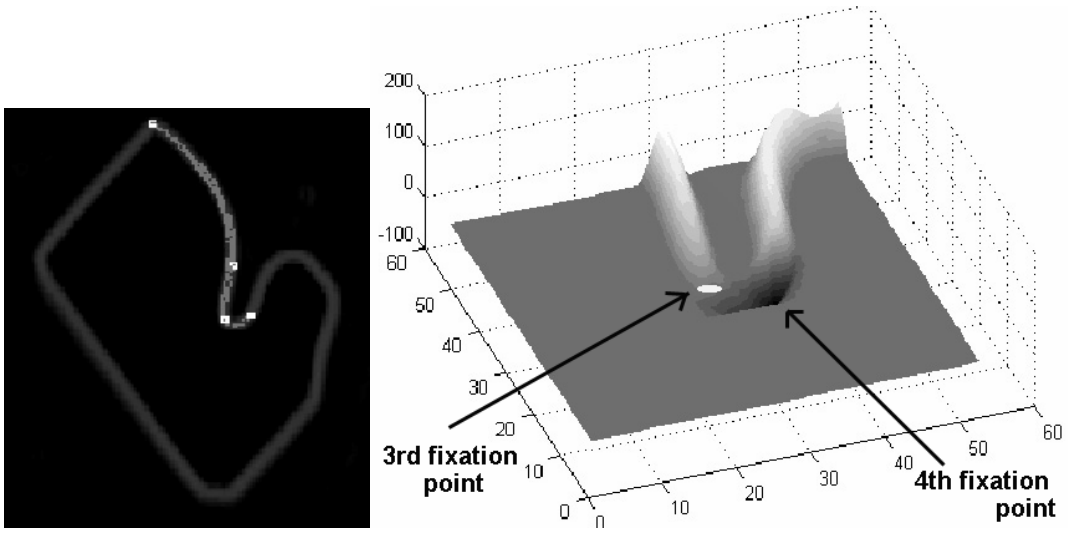

FIGURE 4.7 (a) Path leading to 4th fix. pt. (b) $F_1(x; x^3)$ surface.

First, note that fixation points are not uniformly distributed. Along the contour of the object they are found at critical points where directional cue begins to change. The faster the directional cue changes, the more closely the fixation points are located. Also, we observe that the path leading to next fixation point is along the outline due to the β_{11} term that marks background points where the image gradient vanishes as obstacles and it grows along the saccade direction due to the β_{12}. However, this path is jagged and winding as there is a trade off between smoothness and preferred saccade direction.

4.1.2. Tracing Based on Fixation Points

Through Figures 4.8-4.10, tracing of outline of first few fixation points and potential field surfaces around those fixation points are shown. In leftmost figures, the thinner trajectory - tracing the object's outline and ending up at the next fixation point is generated. The values of m and n are 1 and 0.1 respectively. In rightmost figures, $F_2(x; x^{k+1})$ surfaces for a fixed x^{k+1} are shown. Because the point x^{k+1} is a stable critical point of F_2, it occurs in the dark region as minima of $F_2(x; x^{k+1})$ as expected - i.e. the local minima of $F_2(x; x^2)$ surface in Figure 4.8(b) indicates location of 2rd fixation point. In all

rightmost images, the conic potential due to γ_2 is hollowed out at regions where image gradient does not vanish.

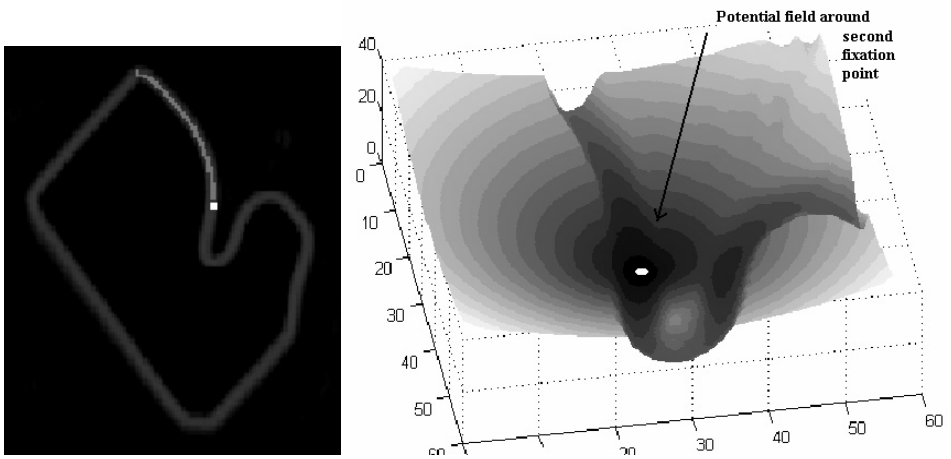

FIGURE 4.8 (a) Thinner path generated between x^1 and x^2. (b) $F_2(x; x^2)$ surface.

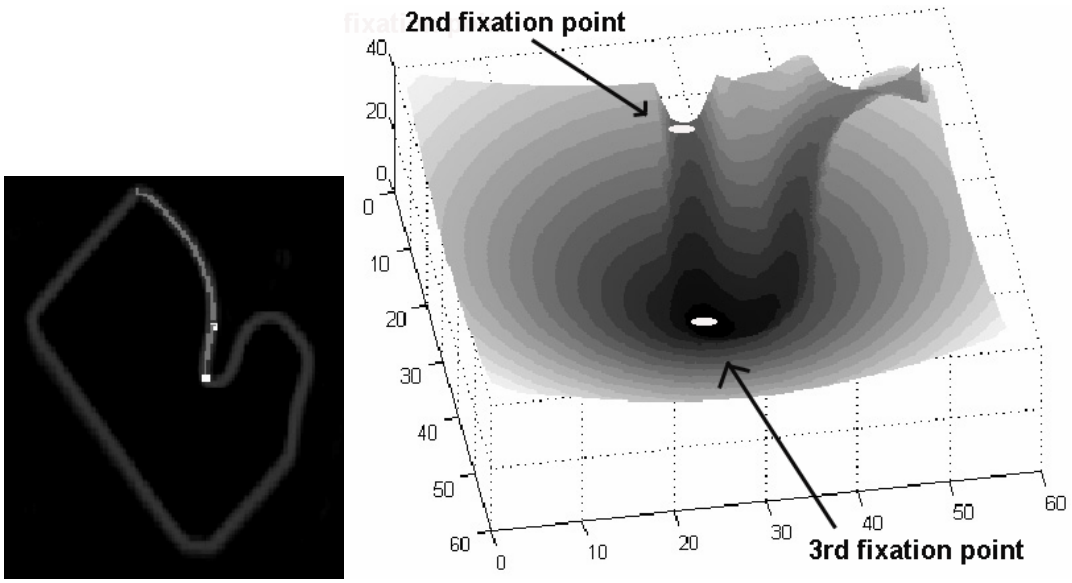

FIGURE 4.9 (a) Thinner path generated between x^2 and x^3. (b) $F_2(x; x^3)$ surface.

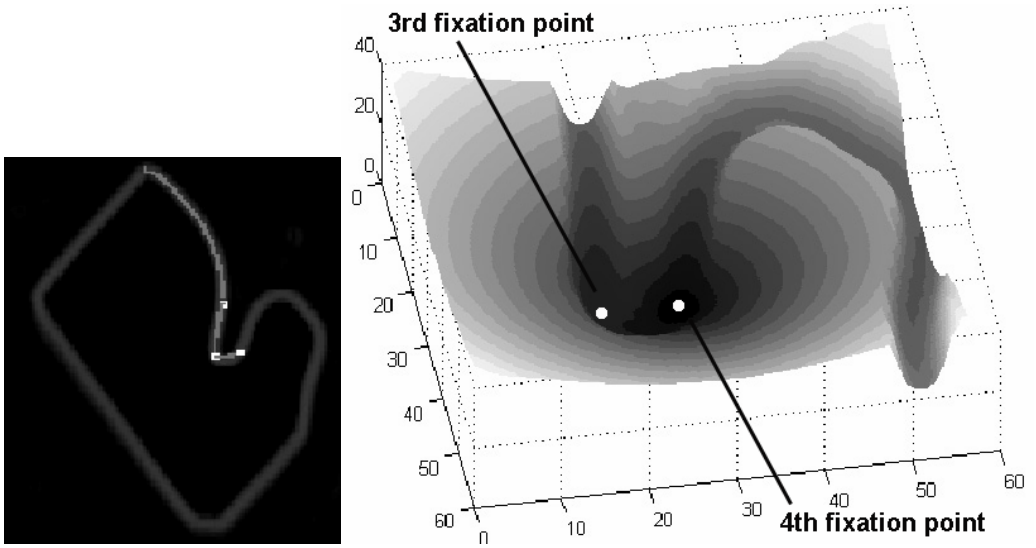

FIGURE 4.10 (a) Thinner path generated between x^3 and x^4. (b) $F_2(x; x^4)$ surface.

4.2. Experiments on Industrial Objects with Different Lighting Conditions

This set of experiments is held on industrial objects with different illumination conditions. First, outline of the object -appropriate for shape parameter computation- is constructed by the approach described in this thesis. Then the shape invariants of the outline are computed for the object. This is done once for an ideally shaped object and stored in the library as the model. Afterwards, shape invariants are computed for every incoming *arbitrarily* oriented object. Let the shape invariants of incoming object be denoted by I_i^O where i=1,..,N – here N stands for number of shape invariants- and that of model by I_i^M. The SID is defined by Shape Invariant Deviation,

$$SID = \frac{1}{N}\left[\sum_{i=1}^{N}\frac{\left(I_i^M - I_i^O\right)^2}{\left(I_i^M\right)^2}\right]^{1/2} \qquad (4.1)$$

We performed three sets of experiments with the objects being illuminated 1) from four sides and 2) then from one side only.

4.2.1. Experiments on Industrial Object-2 with Good Lighting Conditions

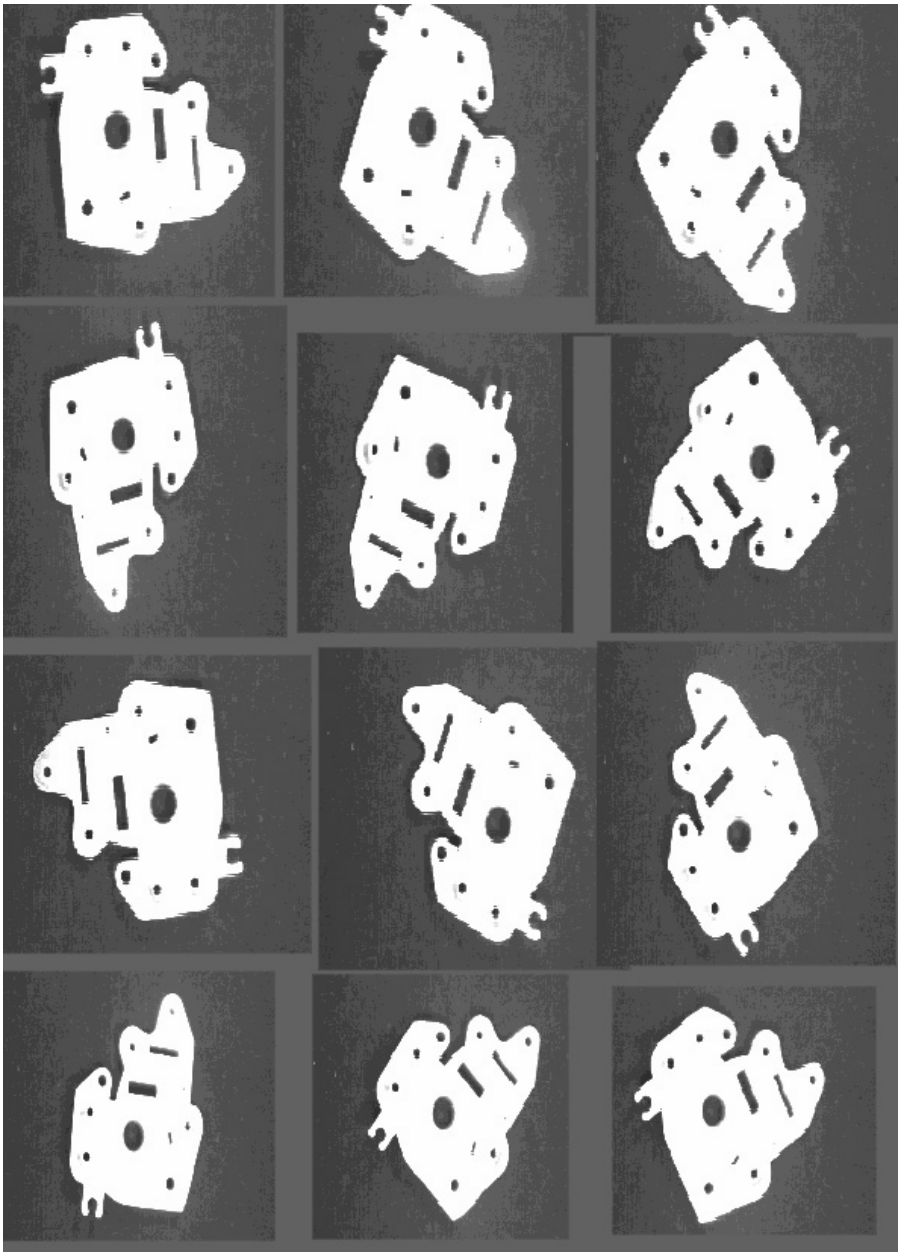

FIGURE 4.11 Images of Part-2 taken at different orientations. The object was illuminated from four sides.

In Figure 4.11, images of industrial part-2 taken at different orientations between zero and 360 degrees are shown. Industrial part is illuminated from four sides to avoid shadowing effects. Although the part is not planar, it seems like planar due to illumination.

Experiments for different orientations of part-2 are held. After having preprocessed, the contour of the object is extracted with the approach presented in this thesis. In order to construct a correct shape model of the part, a crucial practical issue was to compensate for the distortion caused by 4:3 aspect ratio of the imaging system. Although the images in Figure 4.11 all belong to the same part, they are mapped as squeezed and seen to be of a different shape. As our parts are randomly oriented , shape distortion due to unequal aspect ratio should be compensated for. Our solution to this problem is the adaptation of the computation of the EFD coefficients via manipulating equations (2.2)-(2.5) to account for the aspect ratio. Through Figures 4.12 - 4.14, this compensation is illustrated. In Figure 4.12.(a), the contour shape constructed by our approach is shown. Then out of compensated EFD parameters computed for that contour, reconstructed contour of the part is shown in Figure 4.12.(b). Note that through Figures 4.12 (a) - 4.14 (a), although all belong to industrial part-2, they look different, whereas reconstructed contours in 4.12 (b)-4.14(b) look similar, which is very important for inspection purposes.

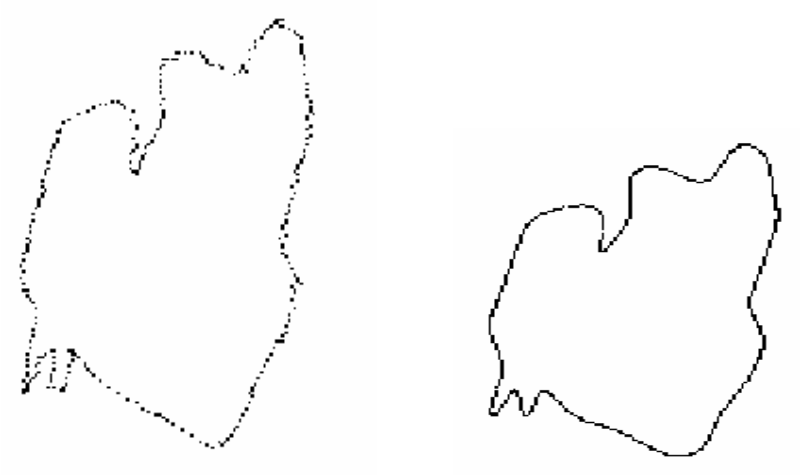

FIGURE 4.12 (a) Contour constructed for part-2 oriented at 45.1 degrees with presented approach, and (b) contour reconstructed out of compensated EFD coefficients obtained from the contour in (a).

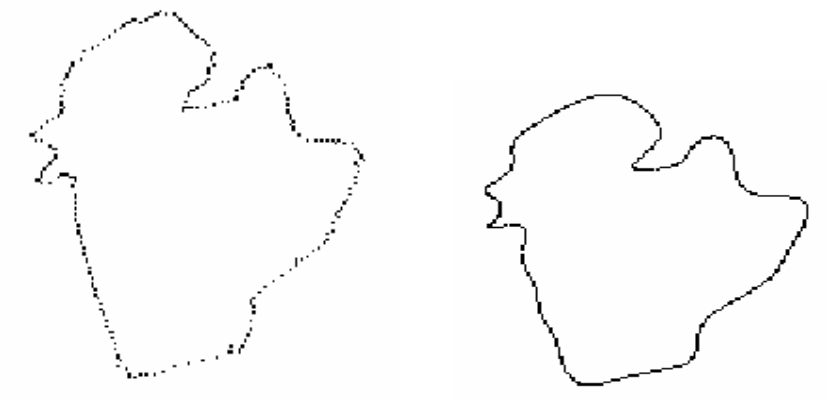

FIGURE 4.13 (a) Contour constructed for part-2 oriented at 10.8 degrees with presented approach, and (b) contour reconstructed out of compensated EFD coefficients obtained from the contour in (a).

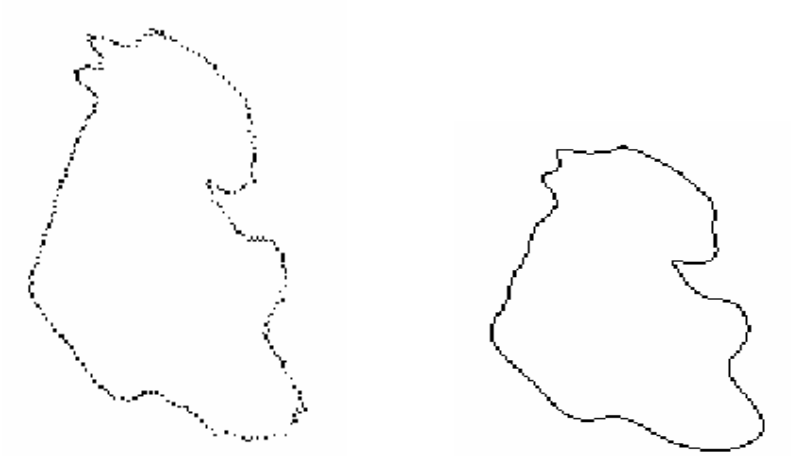

FIGURE 4.14 (a) Contour constructed for part-2 oriented at 295.6 degrees with presented approach, and (b) contour reconstructed out of compensated EFD coefficients obtained from the contour in (a).

Using compensated EFD parameters, shape invariants of the part are computed. These invariants are major and minor axis lengths of fitting ellipse for each harmonic. In table 4.1, shape invariants upto five harmonics for different orientations of part-2 are

illustrated. Each row, represents average values for five experiments at that orientation. Let I^{o}_{2n} and I^{o}_{2n-1} be the major and minor axis lengths of the fitting ellipse of the incoming part for the n^{th} harmonic where n=1..N. Let I^{M}_{2n} and I^{M}_{2n-1} be the major and minor axis lengths of the fitting ellipse of model part for the n^{th} harmonic.

TABLE 4.1 EFD shape invariants of part-2 computed upto fifth harmonics at different orientations with good lighting conditions.

Orientation	I_1^o	I_2^o	I_3^o	I_4^o	I_5^o	I_6^o	I_7^o	I_8^o	I_9^o	I_{10}^o
10,87	27,63	35,89	1,41	5,89	0,48	5,35	1,97	3,28	0,32	1,21
45,12	28,10	35,22	1,14	6,16	0,86	4,93	1,94	2,87	0,46	1,57
100,37	26,56	35,66	3,13	6,06	0,91	5,82	1,47	3,40	0,32	1,87
124,84	26,70	36,51	2,27	5,74	0,32	4,53	2,04	3,70	0,59	0,92
155,69	27,12	35,50	2,87	6,56	0,68	4,72	2,04	3,52	0,56	1,08
171,53	27,49	35,45	2,17	6,37	0,67	4,86	2,03	3,31	0,58	1,09
196,85	27,05	35,44	2,27	6,42	0,52	4,95	1,66	3,19	0,49	1,41
219,89	27,83	33,96	2,48	7,82	1,24	4,59	1,42	2,60	0,25	1,34
241,60	28,13	35,67	1,48	5,91	0,27	4,41	1,16	2,79	0,82	1,37
295,62	26,78	35,76	3,75	6,86	0,53	4,86	1,29	3,57	0,32	1,38
330,18	27,40	35,32	2,88	6,91	0,39	4,44	1,63	3,00	0,23	1,01
346,80	27,17	35,36	2,94	6,79	0,77	4,83	2,37	3,10	0,44	1,03
Min:	26,56	33,96	1,14	5,74	0,27	4,41	1,16	2,60	0,23	0,92
Max	28,13	36,51	3,75	7,82	1,24	5,82	2,37	3,70	0,82	1,87
Model	I_1^M	I_2^M	I_3^M	I_4^M	I_5^M	I_6^M	I_7^M	I_8^M	I_9^M	I_{10}^M
9,58	27,27	36	2,3	6,26	0,42	5,21	2,14	3,16	0,36	1,04

The part oriented at 9.58 degrees is assigned to be the model part. Deviation in shape invariants for the incoming parts at different orientations compared to that of model

part are computed by SID equation defined in (4.1). In Figure 4.15, maximum, minimum and average values of SID are displayed. SID values are less than one percent.

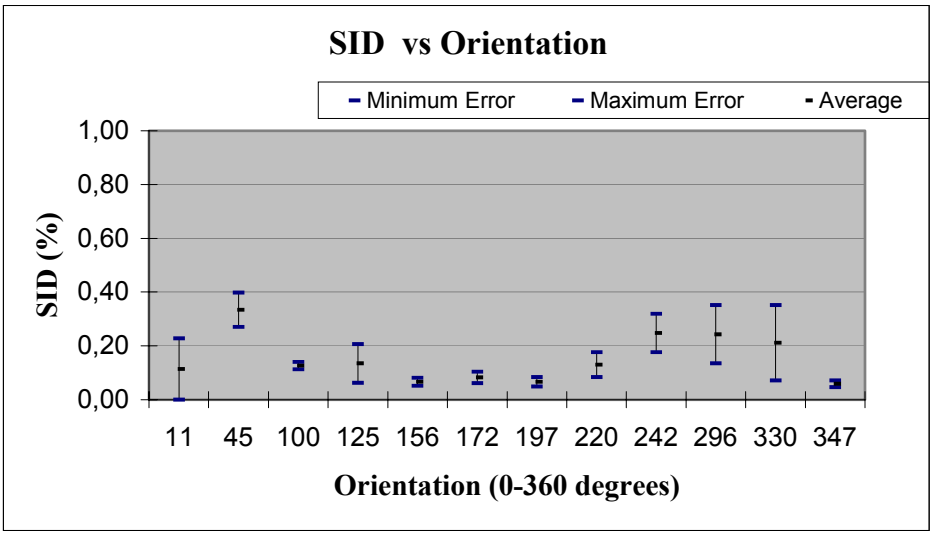

FIGURE 4.15 SID values for shape invariants of incoming part at different orientations. Error is computed with respect to the invariants of model part.

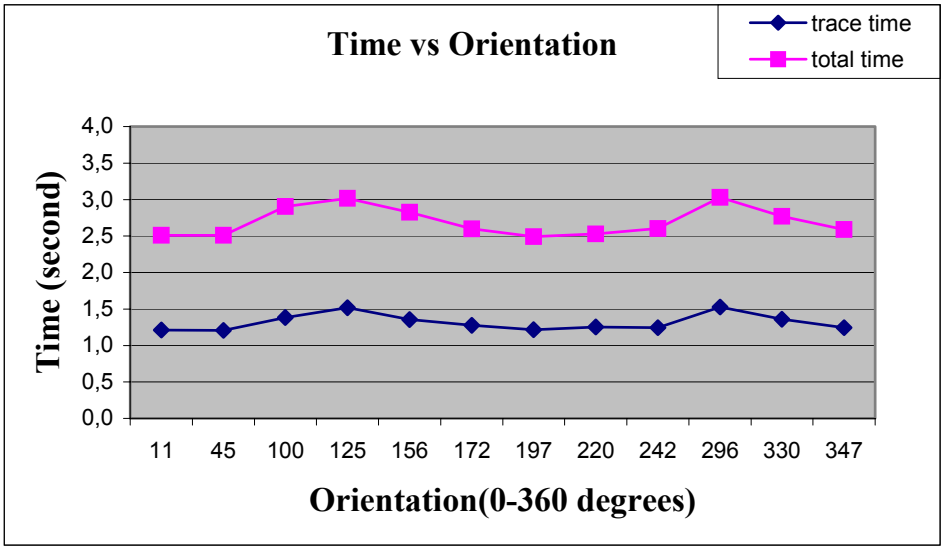

FIGURE 4.16 The time duration of our approach and whole processing.

Considerations related with time are illustrated in Figure 4.16. The duration of processing that only includes generation of fixation points and contour tracing is displayed as trace time. The duration of processing that includes preprocessing, generation of fixation points, contour tracing and shape parameters computation is displayed as total time. Tracing time is around 1.0-1.5 seconds, whereas total processing time is around 2.5-3.0 seconds. Note that the difference between total time and tracing time –duration of processing that includes preprocessing and shape parameters computation- is almost constant, 1.5 seconds, as expected.

4.2.2. Experiments on Industrial object-1 with Good Lighting Conditions

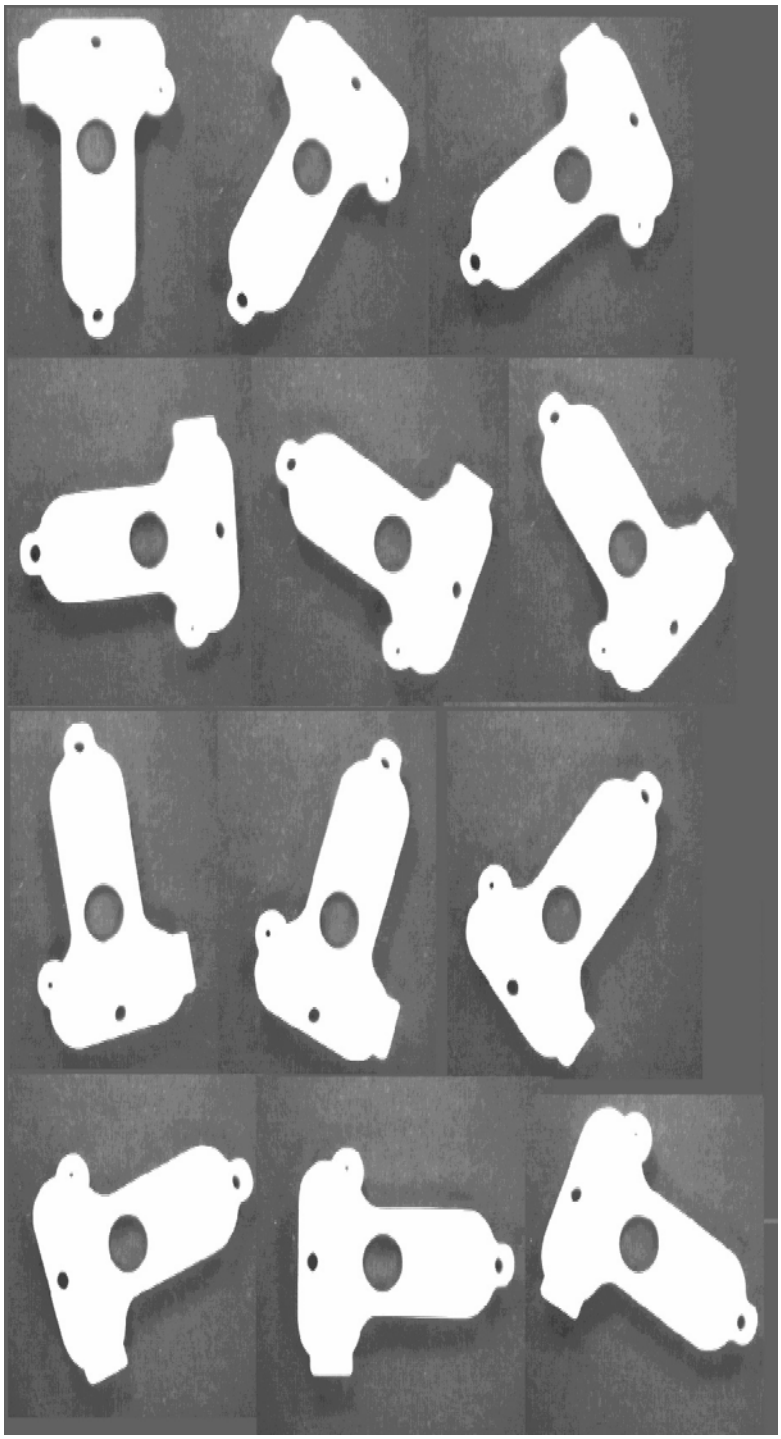

FIGURE 4.17 Images of Part-1 taken at different orientations. The object was illuminated from four sides.

In Figure 4.17, images of industrial part-1 taken at different orientations between zero and 360 degrees are shown. The industrial part is illuminated from four sides to avoid shadowing effects. Experiments for different orientations of part-1 are held. Through Figures 4.18(a) - 4.20(a), contour of part-1 obtained by our approach is illustrated. Through Figures 4.18 (b) - 4.20 (b), reconstructed contours are displayed.

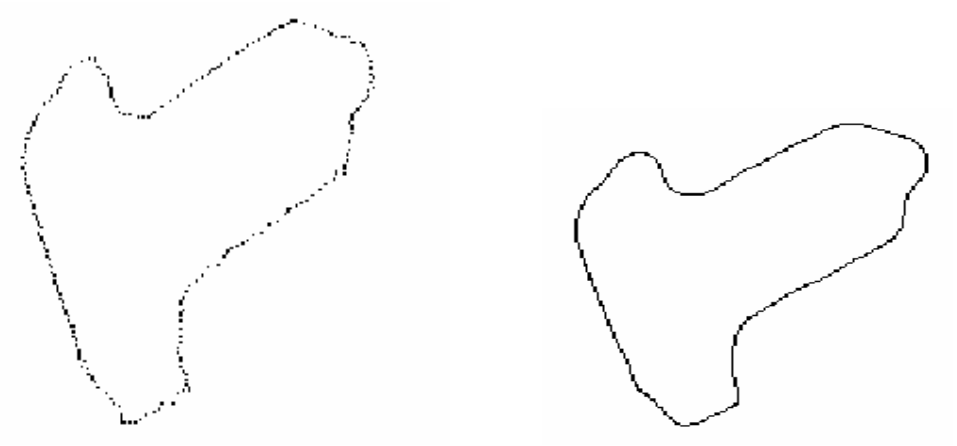

FIGURE 4.18 (a) Contour constructed for part-1 oriented at 26.86 degrees with presented approach, and (b) contour reconstructed out of compensated EFD coefficients obtained from the contour in (a).

FIGURE 4.19 (a) Contour constructed for part-1 oriented at 328.51 degrees with presented approach, and (b) contour reconstructed out of compensated EFD coefficients obtained from the contour in (a).

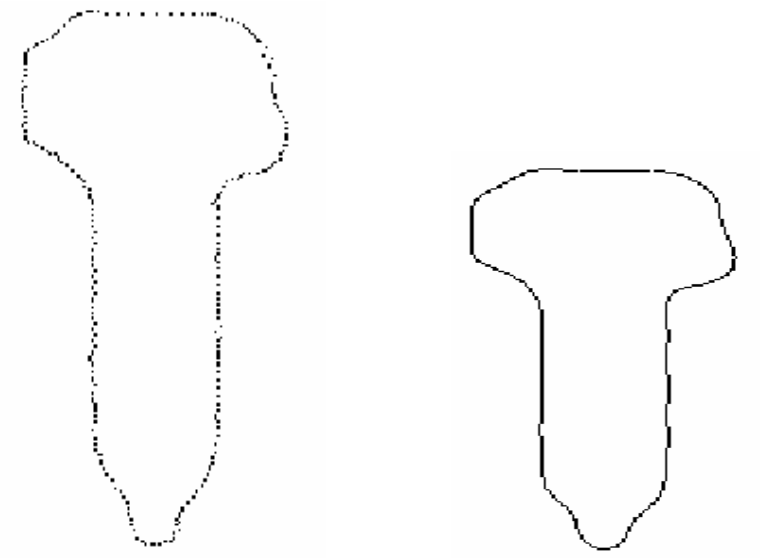

FIGURE 4.20 (a) Contour constructed for part-1 oriented at 278.33 degrees with presented approach, and (b) contour reconstructed out of compensated EFD coefficients obtained from the contour in (a)

Using compensated EFD parameters, shape invariants of the part are computed. In table 4.2, shape invariants upto five harmonics for different orientations of part-1 are illustrated. Each row, represents average values for five experiments at that orientation. The part oriented at 4.12 degrees is assigned to be the model part. Deviation in shape invariants for the incoming parts at different orientations compared to that of model part are computed according to the SID equation in (4.1). In Figure 4.21, maximum, minimum and average values of SID are displayed. SID values are less than one percent.

TABLE 4.2 EFD shape invariants of Part2 computed upto fifth harmonics at different orientations with good lighting conditions.

Orientation	I_1^o	I_2^o	I_3^o	I_4^o	I_5^o	I_6^o	I_7^o	I_8^o	I_9^o	I_{10}^o
4,11	27,35	43,37	6,06	7,32	3,57	4,80	1,22	3,20	1,01	1,34
26,86	26,86	43,97	5,95	6,86	2,96	4,53	1,22	3,13	1,08	1,80
59,20	26,79	43,68	4,87	7,73	3,51	6,74	0,84	2,05	0,39	1,59
94,41	26,59	44,37	4,29	7,59	3,57	7,12	0,70	1,53	0,29	1,80
137,25	26,39	43,66	3,68	8,51	3,75	6,56	0,54	1,69	0,46	2,18
158,91	27,08	44,04	5,63	7,39	3,52	5,32	0,80	2,49	0,83	1,78
186,61	27,00	44,32	5,96	7,93	3,44	5,39	0,57	2,10	0,84	1,67
208,84	26,64	43,79	5,52	7,37	3,20	5,59	0,56	2,46	1,06	1,86
239,44	26,27	43,72	4,58	7,48	3,38	6,63	0,73	1,93	0,27	1,90
278,33	26,66	43,28	5,06	7,85	3,75	7,22	0,63	1,90	0,26	1,46
264,99	26,46	43,64	4,48	7,68	3,47	6,74	0,59	1,90	0,28	1,94
328,51	27,15	43,94	5,76	7,49	3,28	4,96	1,01	2,98	0,74	1,53
Min:	26,27	43,28	3,68	6,86	2,96	4,53	0,54	1,53	0,26	1,34
Max	27,35	44,37	6,06	8,51	3,75	7,22	1,22	3,20	1,08	2,18
Model	I_1^M	I_2^M	I_3^M	I_4^M	I_5^M	I_6^M	I_7^M	I_8^M	I_9^M	I_{10}^M
4,12	27,27	43	6,55	6,82	3,76	5,02	1,15	3,18	1,19	1,38

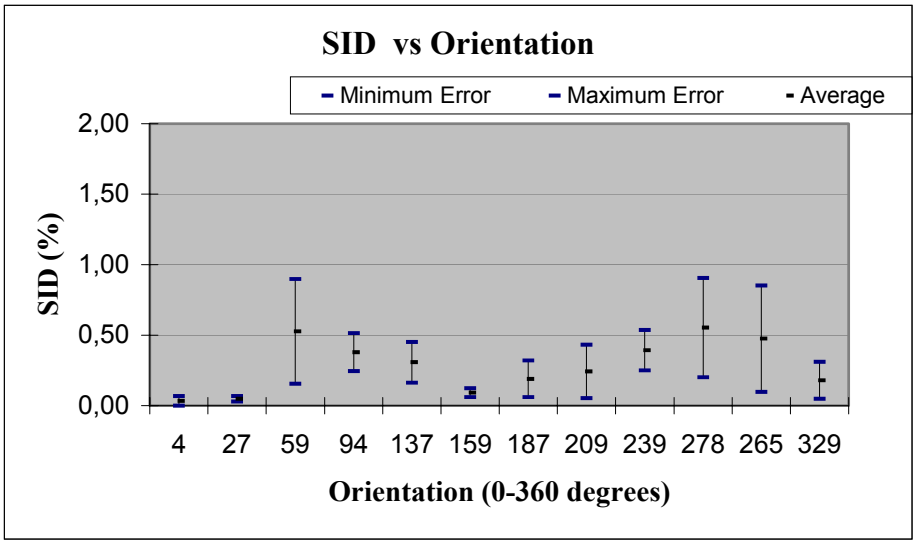

FIGURE 4.21 SID values for shape invariants of incoming part at different orientations. Error is computed with respect to the invariants of model part.

Considerations related with time are illustrated in Figure 4.22. Tracing time is around 1.0-1.5 seconds, whereas total processing time is around 2.5-3.0 seconds. Note that the difference between total time and tracing time –duration of processing that includes preprocessing and shape parameters computation- is almost constant, 1.5 seconds, as expected.

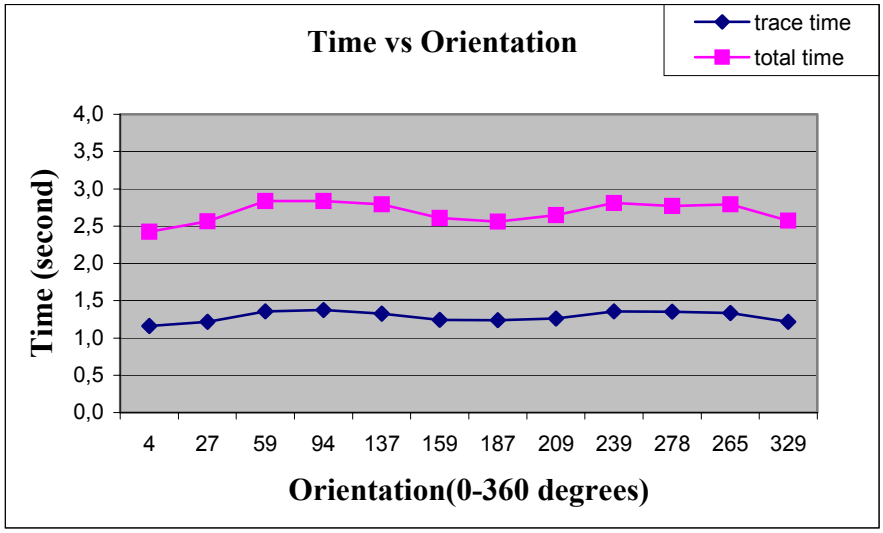

FIGURE 4.22 The time duration of our approach and whole processing.

4.2.3. Experiments on Industrial Object-1 with Directional Lighting

FIGURE 4.23 Images of Part-2 taken at different orientations. The object was illuminated from one side.

In Figure 4.23, images of industrial part-1 taken at different orientations between zero and 360 degrees are shown. The industrial part is illuminated from one side. Experiments for different orientations of part-2 are held. Using compensated EFD parameters, shape invariants of the part are computed. In table 4.3, shape invariants upto five harmonics for different orientations of part-1 are illustrated. Each row, represents average values for five experiments at that orientation.

TABLE 4.3 EFD shape invariants of Part1 computed upto fifth harmonics at different orientations with directional lighting.

Orientation	I_1^o	I_2^o	I_3^o	I_4^o	I_5^o	I_6^o	I_7^o	I_8^o	I_9^o	I_{10}^o
2,08	26,46	43,80	5,83	7,17	2,81	4,86	1,06	2,95	1,23	1,91
29,68	26,70	42,63	4,97	7,70	3,67	6,67	1,02	2,32	0,36	1,44
61,56	26,06	43,75	4,99	7,32	5,54	4,35	4,27	1,82	0,99	1,93
93,76	25,98	43,42	4,68	7,97	3,26	6,38	0,62	2,04	0,40	2,14
137,52	26,18	43,85	5,66	7,30	2,89	5,04	1,00	2,72	0,72	1,86
151,35	25,69	45,11	5,13	7,62	2,36	5,04	0,14	1,66	1,11	2,55
187,48	25,68	44,24	5,41	7,43	2,86	5,19	0,48	1,87	1,03	2,29
203,40	25,94	43,01	4,27	7,32	3,33	7,14	0,49	1,66	0,25	1,79
233,02	25,40	43,50	4,28	7,40	3,19	7,31	0,49	1,25	0,15	1,56
268,65	25,96	43,89	4,99	7,46	3,50	6,63	0,66	1,99	0,22	2,14
308,29	26,01	44,73	4,52	7,43	1,85	5,49	0,74	3,22	0,73	2,14
329,47	26,02	43,62	5,04	7,70	3,10	6,06	0,77	2,14	0,48	2,09
Min:	25,40	42,63	4,27	7,17	1,85	4,35	0,14	1,25	0,15	1,44
Max	26,70	45,11	5,83	7,97	5,54	7,31	4,27	3,22	1,23	2,55
Model	I_1^M	I_2^M	I_3^M	I_4^M	I_5^M	I_6^M	I_7^M	I_8^M	I_9^M	I_{10}^M
1,2	26,39	43,73	6,31	7,03	2,85	4,47	1,36	3,11	1,48	1,65

The part oriented at 1,2 degrees is assigned to be the model part. Error in shape invariants for the incoming parts at different orientations compared to that of model part are computed in three different ways. In Figure 4.24, maximum, minimum and average values of SID are displayed. SID values are less than one percent.

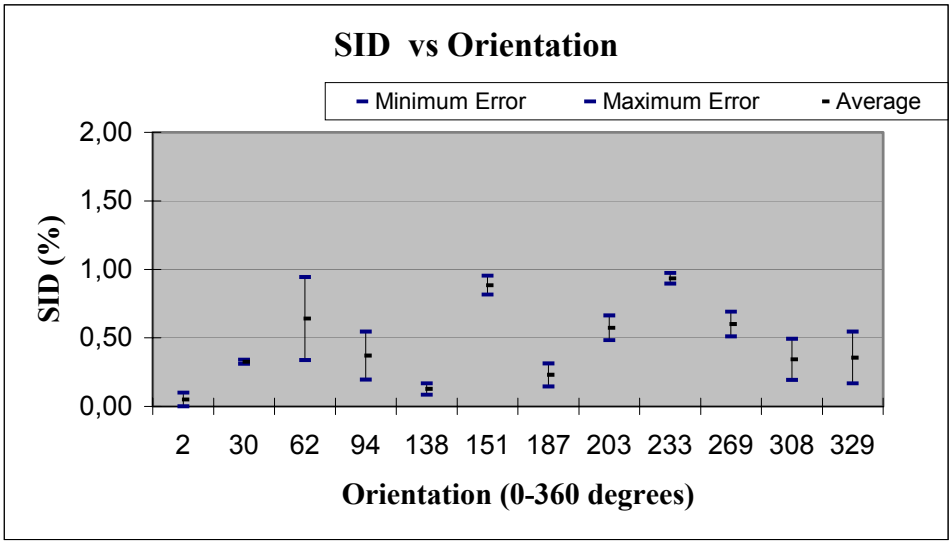

FIGURE 4.24 SID values for shape invariants of incoming part at different orientations. Error is computed with respect to the invariants of model part.

The range of SID values varies between zero and one percent which indicates that there is no significant difference in shape invariants of objects at different orientations. This is because the outline of the object is very well constructed whatever the orientation. Note that as expected, average SID values get slightly larger for the directional lighting case. Moreover, the results indicate the flexibility of the approach under varying lighting conditions. Let us add that the system's performance degrades to some extent in cases where the illumination is changing in a discontinous manner.

Considerations related with time are illustrated in Figure 4.25. Tracing time is around 1.0-1.5 seconds, whereas the total processing time is around 2.5-3.0 seconds. Note that the difference between total time and tracing time –duration of processing that includes pre-processing and shape parameters computation- is almost constant, 1.5 seconds, as expected. Note that there is almost no difference in time performance of our approach on parts illuminated with good lighting conditions and directional lighting.

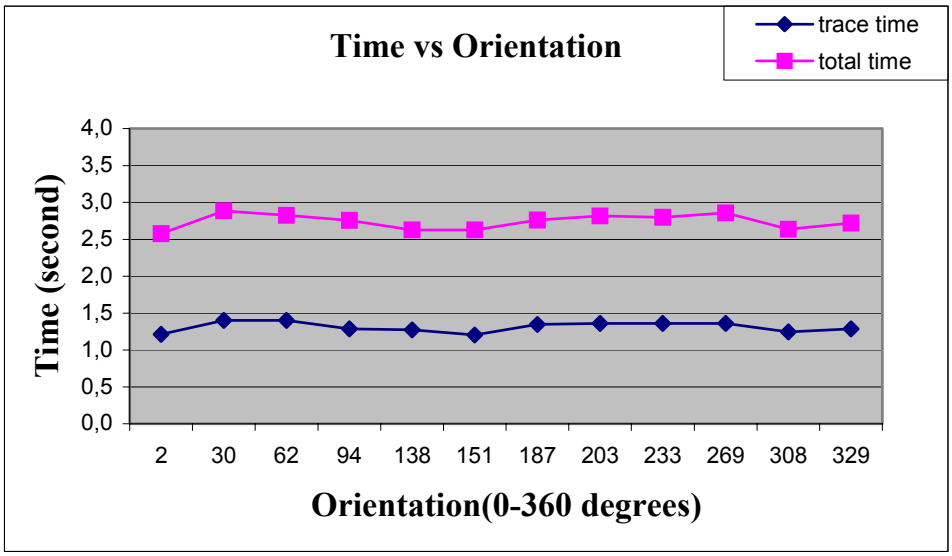

FIGURE 4.25 The time duration of our approach and whole processing experimented on different orientations of part-1 with directional lighting.

5. CONCLUSION AND FUTURE DIRECTIONS

In this thesis, we present a mathematical framework for the generation of fixation points based on artificial potential functions. The heuristic algorithm in our earlier work, which selectively fixates on interesting parts of an incoming image and uses the attentional sequence thus gathered in a task-dependent manner - is formalized. Utilizing this formalism, a sequence of fixation points is generated which are then used to drive the camera actuators. The attentional sequence thus generated is used in a top-down driven task - namely the tracing of an object's outline.

This formalism tantamounted to a feedback based approach such as the tracing of salient parts of the objects. Formulation of the approach in a mathematical framework based on artificial potential functions allows the investigation of the provable correctness of the closed loop system. In this thesis, we have proved that the potential functions constructed admit non-degenerate local minima provided that related parameters are appropriately selected. In determination of the optimal values for the parameters related with these functions, the theoretical results presented are utilized.

We implemented the presented mathematical framework within the visual system of the BUVIS- a visual inspection station developed within our laboratory. Selective perceptual processing thus achieved results in promising real-time behavior in visual inspection of manufactured parts**.** Whole visual data is processed only for preprocessing part of the visual processing and selected regions are only subjected to rest of the processing. Time considerations suggest that it is possible to realize a real-time system using the presented approach. We implemented our approach on Smarteye system which is designed around Texas Instruments DSP chip (TMS320C31PQL). The advances in microprocessors technology evolve in a speed hard to keep up with. Better time performance can be achieved with advanced microprocessors. Computationally intensive parts of the program are directly programmed in TI assembly language. The remaining parts are programmed in C and then cross-compiled to TI assembly code. Computational time can be further reduced if whole visual processing is programmed in assembly language.

Modelling the selective visual processing of the system based on artificial potential functions increased the robustness of the system. We tested the performance of our system

with different illumination conditions. As well as the parts being illuminated from four sides, our system had good inspection performance on parts illuminated with directional lighting. Experimental results indicate the flexibility of the approach under varying lighting conditions.

Our future work will be directed towards modelling all levels of processing associated with using attentional sequences since the type of processing during attention is determined by the task at hand and is much more detailed in nature than that of the pre-attentive stage. We will further integrate the notion of memory to deal with multiple objects with multiple parts.

REFERENCES

1. Rimey, R. D. and C. M. Brown, Selective attention as sequential behavior: Modelling eye movements with an augmented hidden markov model, Technical report, University of Rochester, Computer Science Department, February 1990.

2. Abbott, A. L., "A survey of selective fixation control for machine vision," *IEEE Journal on Control Systems*, Vol. 12, No. 4, pp. 35-54, 1992.

3. Swain, M. J. and M. A. Stricker, "Promising directions in active vision," *International Journal of Computer Vision*, Vol. 11, No. 2, pp.109-126, 1993.

4. Aloimonos, J., "Purposive and Qualitative active vision," In *Proceedings of Image Understanding Workshop*, pp. 101-107, September 1990.

5. Stark, L. and S. R. Ellis, "Scanpaths Revisited: Cognitive Models Direct Active Looking," in Fisher, Monty and Senders (Eds.), *Eye Movements: Cognition and Visual Perception*, pp. 193-226, Erlbaum, 1981.

6. Barrow, H. and J. M. Tenenbaum, "Computational Vision," *Proceedings of IEEE*, Vol. 69, pp. 572-575, 1981.

7. Yalçın, H. and I. Bozma, "An Automated Inspection System with Biologically Inspired Vision," *Proceedings of IROS'98*, pp. 1808-1814, Victoria, CANADA, 1998.

8. Yalçın, H., I. Bozma and M. Tezol, "BUVIS-A Novel Approach to Real-Time Automated Visual Inspection," *Proceedings of Texas Instruments DSP Challenge- Top 20 European Papers*, pp. 9-15, 1998.

9. Yalçın, H. and I. Bozma, "Dairesel Nesnelerin Seçici Algı Kullanılarak Tespit Edilmesi," *Sinyal İşleme ve Uygulamaları Kurultayı- SIU'97 Bildiriler Kitabı*, Kuşadası, pp.272-277, Turkey, 1997.

10. Ballard, D. H. and A. Ozcandarlı, "Eye Fixation and Early Vision: Kinetic Depth," *Proceedings of Second International Conference on Computer Vision*, pp. 524-531, December 1998.

11. Ballard, D. H., "Animate Vision," *Artificial Intelligence*, Vol. 48, pp. 57-86, 1991.

12. Gouras, P., "Oculomotor System," in J.H. Schwartz and E.R.Kandel (Eds.), *Principles of Neural Science*, Elsevier, 1986.

13. Kelly, J. P., "Anatomy of Central Visual Pathways," in J.H. Schwartz and E.R.Kandel (Eds.), *Principles of Neural Science*, Elsevier, 1988.

14. Noton, D. and L. Stark, "Eye Movements and Visual Perception," *Scientific American*, 224(6), 1971.

15. Kowler, E., *Eye Movements and Their Role in Visual and Cognitive Processes*, Elsevier, 1990.

16. Hubel, D. H., *Eye Brain and Vision*, Scientific American Lib., 1988.

17. Koch, C. and S. Ullman, Selecting One Among the Many: A Simple Network Implementing Shifts in Selective Visual Attention, M.I.T. AI Memo 770, 1984.

18. Yeshurun, Y. and E. L. Schwartz, "Shape Description with a Space-variant Sensor," *IEEE Transactions on Pattern Analysis and machine Intelligence*, Vol. 11, pp. 1217-1222, 1989.

19. Soyer, Ç., H. I. Bozma, and Y. Istefanopulos, "Biologically Motivated Vision System," *Proceedings of IROS'96*, pp. 680-687, JAPAN, 1996.

20. Soyer, Ç. and H. I. Bozma, "Furher Experiments in Classification of Attentional Sequences: Combining Instantaneous and Temporal Evidence," *Proceedings of ICAR'97*, pp. 991-995, California, USA, 1997.

21. Westin, C. F., "Attention Control for Robot Vision," *Proceedings of CVPR'96*, pp. 726-732, 1996.

22. Fiala, J., R. Lumia, K. J. Roberts and A.J. Wavering, "TRICLOPS: A Tool For Studying Active Vision," *International Journal of Computer Vision*, Vol. 12, No. 2, pp. 231-250, 1994.

23. Clark, J. J. and N. J. Ferrier, "Modal Control of an Attentive Vision System," *Proceedings of Second International Conference on Computer Vision*, pp. 514-518, December 1988.

24. Rimey, R. and C. Brown, "Control of Selective Perception Using Bayes Nets and Decision Theory," *International Journal of Computer Vision*, Vol. 12, No. 2, pp. 173-207, 1994.

25. Slowe, T. and I. Marsic, "Saliency-Based Visual Representation for Compression," *Proceedings of IEEE International Conference on Image Processing (ICIP'97),* pp. 725-731, Santa Barbara, October 1997.

26. Brown, C., "Selective Perception and Sensor Fusion with Bayes Nets", 1998, http://www.cs.rochester.edu/u/brown/rsta.html.

27. Kennedy, C. W., E. G. Hoffman and S. D. Bond, *Inspection and Gaging*, Industrial Press, New York, 1987.

28. Wilson, D. J., "The Application of AI to aid Defect Classification in an Automated Visual Inspection System", 1998, http://www.ucl.ac.uk/~ucaidjw/h_work.htm.

29. Newman, T. S. and A. Jain, "A Survey of Automated Visual Inspection," *Computer Vision and Image Understanding,* Vol. 61, No. 2, pp. 231-262, March 1995.

30. Batchelor, B. G. and D. W. Braggins, "Commercial Vision Systems," in Torras ed, *Computer Vision Theory and Industrial Applications*, pp.405-452, Springer-Verlag,

New York, 1992.

31. UK Industrial Vision Association, "UKIVA Applications", 1998, http://www.ukiva.org.

32. Khatib, O., "Real-time Obstacle Avoidance for Manipulators and Mobile Robots," *The International Journal of Robotics Research*, Vol. 5, No. 1, pp. 90-99, Spring 1986.

33. Rimon, E. and D. E. Koditschek, "Exact Robot Navigation Functions using Artificial Potential Fields," *IEEE Transactions on Robotics and Automation*, Vol.8, No. 5, pp. 501-518, 1992.

34. Rimon, E., A Navigation Function for a Simple Rigid Body, Technical Report 9014, Yale University, 1990.

35. Koditschek, D. E., "An Approach to autonomous Robot Assembly," *Robotica,* Vol. 12, pp. 137-155, 1994.

36. Krogh, B. H., "A Generalized Potential Field Approach to Obstacle Avoidance Control," *Proceedings SME Conference on Robotics Research*, pp. 441-447, PA, August 1984.

37. Connolly, C. I., J. B. Burns, and R. Weiss, "Path Planning using Laplace's Equation," *Proceedings of IEEE International Conference on Robotics and Automation*, pp. 2102-2106, OH, May 1990.

38. Barraquand, J. and J. C. Latombe, "A Monte-Carlo Algorithm for Path Planning with Many Degrees of Freedom," *IEEE International Conference on Robotics and Automation*, pp.1712-1717, OH, May 1990.

39. Barraquand, J., B. Langlois and J. C. Latombe, "Robot Motion Planning with Many Degrees of Freedom and Dynamic Constraints," *Proceedings of Fifth International Symposium on Robotics Research*, pp. 74-83, Japan, Aug 1989.

40. Warren, C. W., "Global Path Planning using Artificial Potential Fields," *Proceedings IEEE International Conference on Robotics and Automation*, pp. 316-321, AZ, May 1989.

41. Newman, W. S. and N. Hogan, "High Speed Robot Control and Obstacle Avoidance using Dynamic Potential Functions," *Proceedings IEEE International Conference on Robotics and Automation*, pp. 14-24, NC, April 1987.

42. Ahuja, N. and J. Chuang, "Shape Representation Using a Generalized Potential Field Model," *IEEE Transactions on Pattern Analysis and Machine Intelligence*, Vol. 19, No. 2, pp. 169-175, February 1997.

43. Yarbus, A., *Eye Movements and Vision*, Plenum Press, New York, 1967.

44. Lin, C. and C. Hwang, "New Forms of Shape Invariants from Elliptic Fourier Descriptors," *Pattern Recognition*, Vol 20, No. 5, pp.535-545, 1987.

45. Kuhl, F. P., "Elliptic Fourier Features of a Closed Contour," *Computer Graphics and Image Processing*, Vol. 18, pp. 236-258, 1982.

46. Safaee-Rad, R., "Application of Moment and Fourier Descriptors for the Accurate Estimation of Elliptical Shape Parameters," *IEEE Robotics and Automation*, pp.2465-2468, 1991.

47. *TMS320C3x User's Guide: Digital Signal Processing Solutions*. Revision L, Texas Instruments, 1997.

REFERENCES NOT CITED

Ballard, D. H. and C. M. Brown, "Principles of Animate Vision," *CVGIP: Image Understanding*, Vol. 56, No. 1, pp. 3-21, July 1992.

Chandran, S. and A. K. Potty, "Energy Minimization of Contour Using Boundary Conditions," *IEEE Transactions on Pattern Analysis and Machine Intelligence*, Vol.20, No. 5, pp. 546-549, May 1998.

Henderson, J. M., "Visual Attention and Attention-Action Interface," in K. Akins (Eds.), *Perception*, pp. 290-316, Oxford University Press, 1996.

Kass, M., A. Witkin and D. Terzopoulos, "Snakes: Active Contour Models," *International Journal of Computer Vision*, Vol. 1, No. 4, pp. 321-331, 1987.